Volume 48, Number 3, 2022.

Mobility & Vehicle Mechanics

International Journal for Vehicle Mechanics, Engines and Transportation Systems

ISSN 1450 - 5304

UDC 621 + 629(05)=802.0

UNIVERSITY OF KRAGUJEVAC, FACULTY OF ENGINEERING December, 2022.

M V M **M**obility **V**ehicle **M**echanics

*Editors: Prof. dr **Jovanka Lukić**; Prof. dr **Čedomir Duboka***

MVM *Editorial Board*
University of Kragujevac
Faculty of Engineering
Sestre Janjić 6, 34000 Kragujevac, Serbia
Tel.: +381/34/335990; Fax: + 381/34/333192

For Publisher: Prof. dr Slobodan Savić, dean, University of Kragujevac, Faculty of Engineering

Publishing of this Journal is financially supported from:
Ministry of Education, Science and Technological Development, Republic Serbia

Mobility & **M**otorna

Vehicle **V**ozila

Mechanics **M**otori

Volume 48
Number 3
2022.

Mobility & **V**ehicle **M**echanics

Motorna **V**ozila **M**otori

Volume 48
Number 3
2022.

MOBILITY & VEHICLE MECHANICS

https://doi.org/10.24874/mvm.2022.48.03.01
UDC:621.43.056

THE INDICATOR DIAGRAMS IN P-V COORDINATES CALCULATED AND MEASURED ON THE ENGINE STAND

Vasile Blaga [1], Mihai Blaga [2]*

Received in June 2022 *Revised in July 2022* *Accepted in August 2022*

RESEARCH ARTICLE

ABSTRACT: This paper presents the numerical results of a simulation of the thermodynamic cycle for in spark ignition engine (SI) in normal external conditions (T_0=293 K; p_0=10^5 Pa) and revolution n=5500 rpm, at full charge. The simulation took in account the constraint for λ=1, for air pollution reduction whit combustible gases This paper presents the numerical results of a simulation of the thermodynamic cycle for in spark ignition engine (SI) in normal external conditions (T_0=293 K; p_0=10^5 Pa) and revolution n=5500 rpm, at full charge. The simulation took in account the constraint for λ=1, for air pollution reduction whit combustible gases [1]. The indicator diagram was calculated in p-V coordinates, and in p-α coordinates. Equations for thermal processes that take place in the engine were determined and then entered into a computer program. Using these equations, the state parameters were calculated at the characteristic points of the engine cycle. The research was conducted in order to obtain information that could be used improving the characteristics of an engine SI. The operating mode of the engine is defined by the speed of rotation and load, but it involves knowledge, in addition to these, of the thermal regime (parts temperature, cooling fluid temperature, intake air temperature, exhaust temperature, altitude corrections and etc.). The logic diagram of the calculation program is presented. The calculation program for determining the indicator diagram is done in Mathcad, both for the low pressure area and for the high pressure. The engine stand and the pressure transducer with their characteristics are presented. The diagrams are shown in p-V and p-φ coordinates. The p-V indicator diagrams are calculated by the presented program based on data measured on the engine stand.. The indicator diagram was calculated in p-V coordinates, and in p-α coordinates. Equations for thermal processes that take place in the engine were determined and then entered into a computer program. Using these equations, the state parameters were calculated at the characteristic points of the engine cycle. The research was conducted in order to obtain information that could be used improving the characteristics of an engine SI.

[1]*Vasile Blaga, University of Oradea, Mechanical Engineering and Automotive Department, 1 University Street, Bihor County, Romania, vblaga.ar@gmail.com,* ORCID ID: 0000-0002-6843-9832 *(*Corresponding author)*

[2]*Mihai Blaga, University of Oradea, Mechanical Engineering and Automotive Department, 1 University Street, Bihor County, Romania, mihaiblaga332@gmail.com,* ORCID ID: 0000-0003-1806-2691

The operating mode of the engine is defined by the speed of rotation and load, but it involves knowledge, in addition to these, of the thermal regime (parts temperature, cooling fluid temperature, intake air temperature, exhaust temperature, altitude corrections and etc.). The logic diagram of the calculation program is presented. The calculation program for determining the indicator diagram is done in Mathcad, both for the low pressure area and for the high pressure. The engine stand and the pressure transducer with their characteristics are presented. The diagrams are shown in p-V and p-φ coordinates. The p-V indicator diagrams are calculated by the presented program based on data measured on the engine stand.

KEY WORDS: *thermodynamic cycle, indicator diagram, engine stand, characteristic points, the engine speed, low pressure, high pressure*

INDIKATORSKI DIJAGRAMI U P-V KOORDINATAMA ODREĐENI PRORAČUNOM I MERENJEM NA PROBNOM STOLU

REZIME: U ovom radu su prikazani numerički rezultati simulacije termodinamičkog ciklusa za benzinski motor u normalnim spoljašnjim uslovima (T_0=293 K; p_0=105 Pa) pri broju obrtaja n=5500 o/min i pri punom punjenju. U simulaciji je uzeto u obzir ograničenje za λ=1, kako bi se smanjilo zagađenje produktima sagorevanja [1]. Indikatorski dijagram je izračunat u p-V koordinatama, i u p-α koordinatama. Određene su jednačine za termičke procese koji se odvijaju u motoru, a zatim unete računski program. Koristeći ove jednačine, izračunati su parametri stanja u karakterističnim tačkama ciklusa motora. Istraživanje je sprovedeno u cilju dobijanja informacija koje bi mogle da se koriste za poboljšanje karakteristika motora SI. Režim rada motora je definisan brojem obrtaja i opterećenjem, ali podrazumeva poznavanje, pored ovih, i toplotnog režima (temperatura delova, temperatura rashladne tečnosti, temperatura usisnog vazduha, temperatura izduvnog gasa, korekcije nadmorske visine itd.) [1]. Prikazan je algoritam programa za proračun indikatorskog dijagrama. Programski paket je razvijen u Mathcad okruženju i namenjen je za određivanje indikatorskog dijagrama kako u području niskog pritiska, tako i u području visokog pritiska. Predstavljen je probni sto sa motorom i davačima pritiska odgovarajućih karakteristika. Proračunati dijagrami su prikazan u p-V i p-φ koordinatama. Dijagrami prikazani u p-V koordinatama se, računaju pomoću razvijenog programa i na bazi izmerenih veličinama na motoru određena su odstupanja proračuna i merenja.

KLJUČNE REČI: *termodinamički ciklus, indikatorski dijagram, optini motor, karakteristične tačke, broj obrtaja, nizak pritisak, visok pritisak*

THE INDICATOR DIAGRAMS IN P-V COORDINATES CALCULATED AND MEASURED ON THE ENGINE STAND

Vasile Blaga, Mihai Blaga

INTRODUCTION

1. THE MODEL CALCULATION FOR CYCLE THERMODYNAMIC DIAGRAM P – V

The mathematical equations of transformation that make up the thermodynamic cycle after which spark-ignition engines run are [2], [6]:

The polytrophic compression a-c:

$$p = p_a \cdot \left(\frac{V_a}{V}\right)^{n_c};\ \mathrm{V} \in [V_a; V_c] \tag{1}$$

$$V_a = V_c + V_s = \frac{V_s}{\varepsilon - 1} + V_s \tag{2}$$

The isochors burn c-z:

$$p = \alpha \cdot p_c\ ; V = V_c = ct. \tag{3}$$

The polytrophic relaxation z-u:

$$p = p_z \cdot \left(\frac{V_z}{V}\right)^{n_u};\ \mathrm{V} \in [V_c; V_u];\ \mathrm{V}_u = \delta \cdot V_c \tag{4}$$

The polytrophic relaxation u-d:

$$p = p_u \cdot \left(\frac{V_u}{V}\right)^{n_d};\ \mathrm{V} \in [V_u; V_d];\ \mathrm{V}_d = V_{d_1} = V_a \tag{5}$$

The freely evacuation d-d_1:

$$p = p_{d1}\ ; V = V_a \tag{6}$$

The forced evacuation d_1-r:

$$p = p_{d1}\ ;\ V = V_r = V_c \tag{7}$$

The adiabatic extend to evacuation r-r_1:

$$p = \left(\frac{V_r}{V_{r_1}}\right)^{k_e};\ V_{r_1} = V_r \cdot \left(\frac{p_r}{p_a}\right)^{\frac{1}{k_e}} \tag{8}$$

Admissible at constant pressure r_1-a:

$$p = p_a\ ; V = V_a \tag{9}$$

2. THE SCHEME OF THE FUEL SUPPLY SYSTEM

It is proposed to use the calculation model of the engine SI with gasoline injection, when modeling Renix multipoint electronic injection systems. In Figure 1. The fuel supply scheme of the Renix system used to model the system proposed by the author is presented.

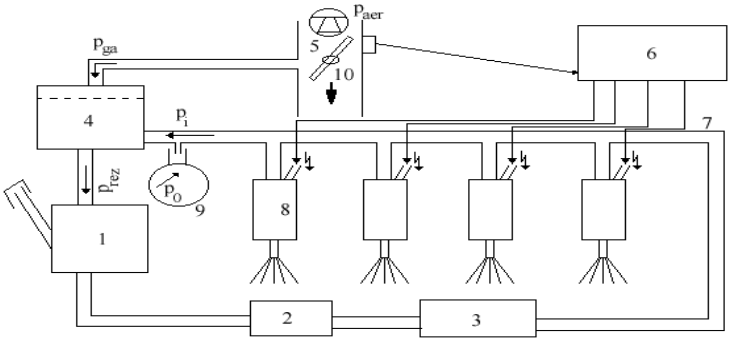

Figure 1 The fuel supply system: 1 – fuel tank; 2 – electric pump; 3 – fuel filter; 4 – pressure regulator; 5 – flowmeter to measure the intake air quantity; 6 – computer; 7 – injection manifold; 8 – electromagnetic injectors; 9 – valve to measure the pressure in the system; 10 – throttle; pair – the environmental pressure; peg – the pressure of the exhaust gases; pi – the injection pressure; ptank – the pressure in the fuel tank

The modelling of the SI engine cycle proposed by the authors is realized by running a computer program. The engine cycle proposed by the authors for the analytical calculus is given in figure 2.

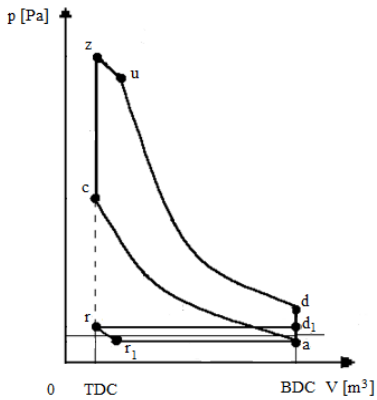

Figure 2 The engine cycle for the analytical calculus

The algorithm for calculating the working gas state parameters at the characteristic points of the engine cycle is presented: point (a) - the end of the intake stroke; point (c) - end of the compression process; point (z) - end of the isochoric combustion process; point (u) - end of the post-combustion process, point (d) - end of the expansion process; point (d1) - end of the free evacuation process; (r) - the end of the forced evacuation process.

The connection between the exhaust valve and the intake valve is made through the isentropic expansion ($r – r_1$). After the opening of the intake valve, the pressure drops from the value corresponding to the pressure of the residual burned gases (p_r) to the value ($p_{r1}=p_a$), equal to the intake pressure (considered to remain constant during the intake

stroke). The pressure during the intake stroke (p_a) is lower than the environmental pressure (p_0) with a value (Δp_a), equal to the total pressure losses inside the intake manifold.

The initial data for the computation are the following: $D = 77 \cdot 10^{-3}$ m; – the cylinder bore; $S = 83{,}6 \cdot 10^{-3}$ m; the piston stroke; $V_s = 0{,}389 \cdot 10^{-3} m^3$; – the swept volume; R=290 J/kg – the working fluid constant; $Q_i = 44 \cdot 10^6$ J/kg; – the net calorific value; L_0=15 kg air/kg fuel – the stoichiometric air requirement; T_0=293 K – the environmental temperature; $p_0 = 1 \cdot 10^5$ Pa – the environmental pressure; λ=1 – the excess air factor; η_{ar}=0,9 – the burning process efficiency; ξ_0=0,8 – the heat release coefficient; ξ_{ga}=2 the gas-dynamic resistance factor of the intake manifold; ρ_0=1,177 kg/m^3 – the intake air density; $d_0 = 0{,}42 \cdot D$[m] – the inner diameter of the intake manifold at the valve port; n=500 … 5500 rot min (with a variation from 100 to 100 rot/min) – the crankshaft rotational speed; [m/s] – the mean piston speed; n_u=0,9 – the polytropic coefficient of the afterburning process; η_p=0,96 – the plenitude coefficient of the engine cycle; $p_r = 1{,}13 \cdot 10^5$ Pa – the residual exhaust gas pressure (the pressure in point r).

The logical scheme for the analytical calculation is presented in figure 4 [3] [4].

3. THE SIMULATE ON COMPUTER AND NUMERICAL RESULT

To can to describe a thermodynamics cycle that is give us for before equation (1 - 9), we must to know the value his nu, nc, nd, ke, α, δ. This size is estimate for normal conditions of temperature and pressure (To=293 K; po=102 kPa) and of revolution of n= 5500 rpm at λ=1, who show the medley character from gaze that are give to burn with pollution products minimum quantitative and qualitative [4].

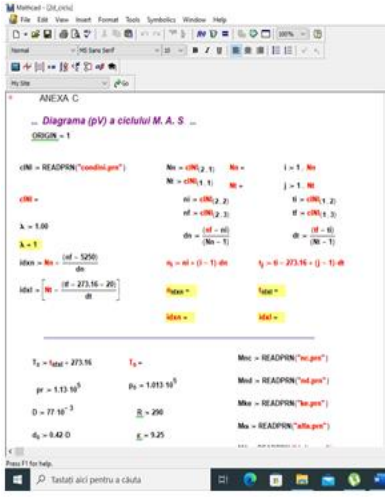

Figure 3 Part of the program with p-V diagram

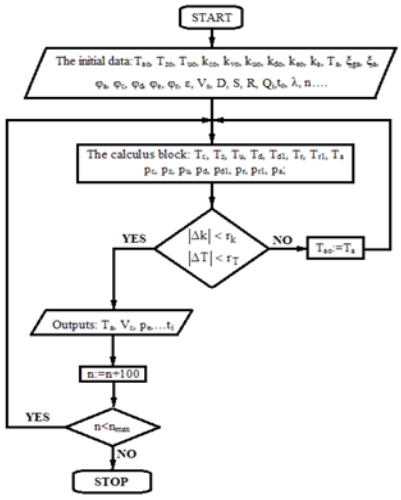

Figure 4 Part of the logic scheme

This the follow numerical for thermodynamics cycle for Engines with Spark Lightning in conditions than work above return it in table 1, figure 5 and 6.

Table 1 *The pressures and the volume in the characteristic points of the engine cyclepoints of the engine cycle*

The point	The pressure (10^5 Pa)	The volume (dm^3)
a	0,8023	0,43615
c	16,4727	0,04715
z	53,9902	0,04715
u	37,9328	0,06979
d	3,5918	0,43615
d_1	1,1300	0,43615
r	1,1300	0,04715
r_1	0,8023	0,06159

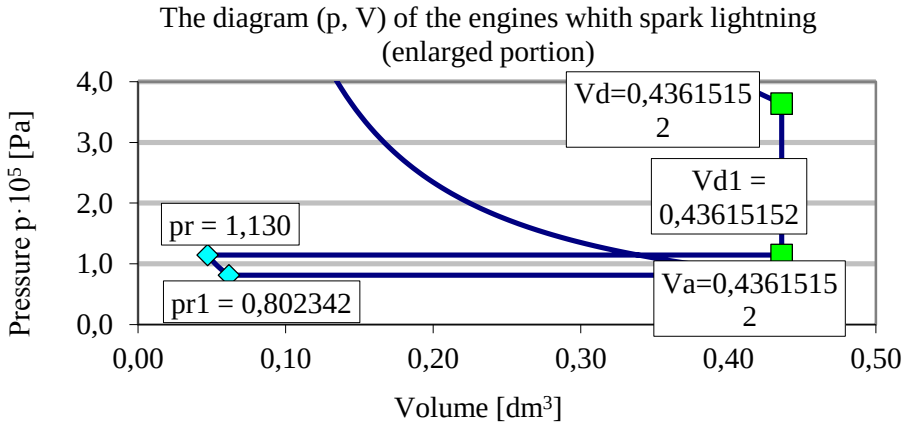

Figure 5 The diagram (p-V) to cycle Engines with Spark Lightning – Enlarged portion

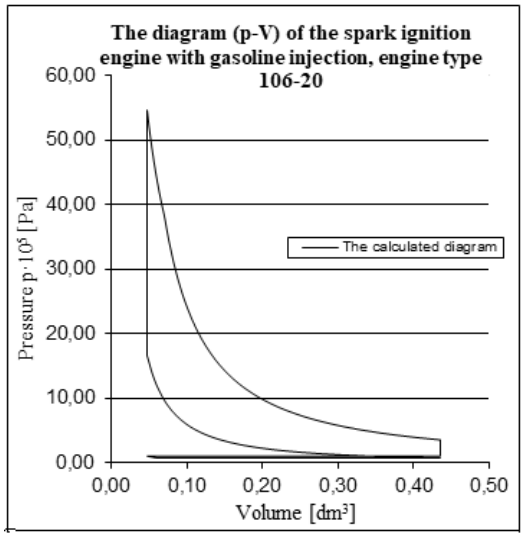

Figure 6 The diagram (p-V) to cycle Engines with Spark Lightning

4. THE MODEL CALCULATION FOR DIAGRAM P-φ

The isentropic expansion r-r1:

$$V_r = V_c\,;\, V_{r1} - V_r = \frac{\pi \cdot D^2}{4} \cdot x_{r1}\,,\ \text{result: } x_{r1} = \frac{V_{r1} - V_r}{S_p};\ \text{where: } S_p = \frac{\pi \cdot D^2}{4}$$
$$\text{The equation of state shows: } p_r \cdot V_r^{k_e} = p_a \cdot V_{r_1}^{k_e};\ \text{result: } V_{r1} = V_r \cdot \left(\frac{p_r}{p_a}\right)^{\frac{1}{ke}} \tag{10}$$

It was noted $\Lambda = r/b$; r- crank length; b- connecting rod length. $\Lambda = 1/3{,}5$. The displacement of the piston is a periodic function of period 2π.

$$x_{r1} = S/2\ \cdot [(1 - cos\varphi) + \Lambda/4\ (1 - \cos 2\varphi)];$$
$$\text{result: } 2x_1/S = (1 - cos\varphi) + (\Lambda/4) - (\Lambda/2) \cdot cos^2\varphi + (\Lambda/4) \tag{11}$$
$$C = (2x_1/S) - (\Lambda/2) - 1\,;\ (\Lambda/2) \cdot cos^2\varphi + cos\varphi + C = 0$$
$$\text{result:}\cos\varphi\ \varepsilon\ [-1;1]\quad \text{result}\ \ \varphi_{r1}$$

$$p = p_r \cdot \left(\frac{V_r}{V_{r1}}\right)^{k_e};\quad x\varepsilon\ [0; x_{r1}];\ \ \varphi\varepsilon\ [0; \varphi_{r1}] \tag{12}$$

The constant pressure inlet r1-a:

$$p = p_a\,; x\varepsilon\ [x_{r1}\,; S];\ \ \varphi\varepsilon\ [\varphi_{r1};\ \pi] \tag{13}$$

The polytropic compression a-c:

$$pp_aV_a^{nc} = pV^{nc};\quad p = p_a\left(\frac{V_a}{V}\right)^{nc};\quad x \in [S; 0];\quad \varphi \in [\pi; 2\pi] \tag{14}$$

V- The instant volume

$$V = V_c + (\pi D^2/4)x_{r1} \tag{15}$$

The isocor combustion c-z:

$$p_z = \alpha \cdot p_c\,;\quad x = 0;\quad \varphi = 0 \tag{16}$$

The polytropic relaxation z-u:

$$V_u - V_c = \frac{\pi \cdot D^2}{4} \cdot x_u\,;\quad x_u = \frac{V_c(\delta - 1)}{S_p};\quad S_p = \frac{\pi \cdot D^2}{4}\,; V_u = \delta \cdot V_c \tag{17}$$
$$cos(\varphi_{1,2}) = \frac{-1 \pm \sqrt{1 - 2\Lambda C}}{\Lambda};\quad x_u = S/2[(1 - cos\varphi) + \Lambda/4(1 - cos2\varphi)]; \tag{18}$$
$$\text{result: } 2x_u/S = (1 - cos\varphi) + \Lambda/4 - (\Lambda/2)cos^2\,\varphi + (\Lambda/4)$$

$$C_1 = (2x_u/S) - (\Lambda/2) - 1\,;\ (\Lambda/2)cos^2\varphi + cos\varphi + C_1 = 0 \tag{19}$$

$$\text{result: } \cos\varphi\varepsilon\ [-1; 1]\cos\varphi\ \varepsilon[-1;1];\ \text{result}\ \varphi_u$$
$$p = p_z \cdot \left(\frac{V_z}{V}\right)^{nu};\ x\varepsilon[0;\ x_u];\quad \varphi\varepsilon[0; \varphi_u] \tag{20}$$

The polytropic destination u-d:

From the equation:

$$p_u \cdot V_u^{nd} = p \cdot V^{nd}$$

$$\text{Result: } p = p_u \cdot \left(\frac{V_u}{V}\right)^{nd}; x \in [x_u; S];\ \varphi \in [\varphi_u; \pi] \tag{21}$$

The free evacuation d-d1:

$$pV_{d1} = V_a;\ \ p = p_{d1} \tag{22}$$

$$p_{d1} = \left(\frac{\varepsilon}{\delta}\right)^{nd} \cdot \delta^{nu};\ \ x = S;\ \ \varphi = \pi \tag{23}$$

The forced evacuation at constant pressure d1-r:

$$p_{d1} = p;\quad x\varepsilon[S;0];\quad \varphi\varepsilon\ [\pi;2\pi]\ \ si\ \ \ p = p_r;\ \ \ x = 0; \varphi = 0 \tag{24}$$

5. THE PROPOSED EXPERIMENTAL MODEL

The main task of the system is to establish the correlation between the engine's intake air mass and the injected fuel mass per cycle, forming a mixture of maximum economy for each engine operating regime. For electronic injection systems, the dependence between the amount of petrol injected per cycle at each engine operating mode and the injector opening time is determined in advance at the test stand, with manually operated control units, according to the criteria of the actual minimum specific fuel consumption, the maximum effective engine torque and the minimum pollutant emissions (carbon monoxide, hydrocarbons, nitrogen oxides), after which it is stored in the computer of the injection equipment, tabular or in the form of curves of variation of the opening time of the injector depending on the speed having as a variable parameter either the depression in the intake manifold or the position of the shutter damper, therefore the pressure transducer existing in these installations must be of special precision.

The adjustment of the amount of petrol injected per cycle for different engine operating modes is based on the amount of air drawn in by means of an air flow meter provided with a transducer which transmits information on the air flow to the computer. Replace the air flow meter with vane and transducer element with a Karman-Vartex type air flow meter based on ultrasonic waves, which improves engine performance. A study is made to choose the excess air coefficient λ; the pressure regulator is modeled; the pressure regulator constant is determined; the electromagnetic injector is modeled and the injection duration ratio is calculated.

Modeling the SI engine with gasoline injection proposed by the author is performed by running a computer program to determine the variation of three-dimensional and two-dimensional parameters in two cases: -dependence on engine speed and excess air coefficient at ambient temperature t_0 = -35… 45ºC and $p_0 = 1 \cdot 10^5$ Pa, in Annex A; [5] -dependence on engine speed and ambient temperature at $\lambda = 1$ and $p_0 = 1 \cdot 10^5$ Pa in Annex B. [5]; Logic of the program for modeling the SI engine with gasoline injection is presented in annex no. 37 [5]. It is proposed to use the model of the pressure regulator and the electromagnetic injector, the model proposed by the author, to determine the mass of fuel injected per cycle and the duration of the injection, with the engine speed and load. The three-dimensional cartographies were made on the computer according to the information provided by different translators and processed on the abscissa, the pressure in the intake

manifold (throttle angle) and the orderly engine speed, the third dimension being the enrichment of the mixture. (injection time) for mapping. injection and ignition advance for the ignition mapping below. Renix multi-point electronic injection system that equips the adapted Dacia Logan Renault engines. The electronic unit is digital and combines two essential functions: ignition and petrol injection. Ignition points and injection time are calculated using the same information (engine speed and absolute pressure in the intake manifold), it makes sense to use a single computer to control the two functions. Among other things, ignition can benefit from additional corrections (water / air temperature) without the use of private translators. In this way, most transducers (speed, pressure, temperature) can be used together for 2 functions, which allows a high degree of reliability without cost compared to two separate computers.

The computer determines the ignition feed angle and the ignition coil contact time. These two pieces of information are emitted in the form of an electrical signal that is transmitted to an ignition power module (MPA), which conducts electricity to the primary coil to regulate the stored energy. A distributor distributes the spark energy to the cylinders. For injection, the central computer simultaneously controls the injectors (one per cylinder) at the same time as the crankshaft rotation, so that they supply each cylinder the same amount of gasoline depending on the amount of air drawn in. The amount of petrol injected depends on the absolute pressure in the intake manifold and the engine speed (crankshaft pressure-speed system). Ignition and injection are determined using information provided by different translators and processed by traversing two 3-dimensional maps, with abscissas (pressure), ordinates (speed), the third dimension is: enrichment of the mixture (or injection time) for injection mapping, figure 7; or the ignition advance for the ignition mapping, figure 8. For each mapping there are, for example, 9 inputs with regularly distributed pressure and 13 inputs with engine speed that does not need equal distribution. In total, therefore, 9 x 13 = 117 theoretical adjustment points are arranged. Writing (9-1) x (13-1) = 96 the elementary surface is made by computer with a double interpolation, with a weighting of each point a defined polygon. The theoretical values of the ignition advance and the duration of the injections are then modulated by corrective parameters: air pressure, air temperature, water temperature, battery voltage, acceleration, noise, etc.

The Renix system applies to multipoint injection or single point injection. It has a modular design, which allows easy and efficient adaptation to different types of 4 - or 6-cylinder engines. It has a self-diagnostic signal that facilitates control, adjustment, troubleshooting operations.

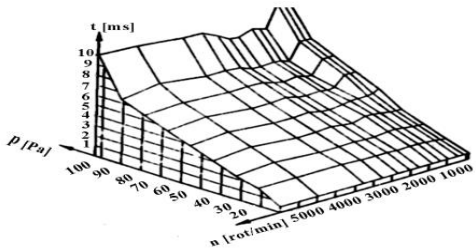

Figure 7 Injection mapping of the Renix

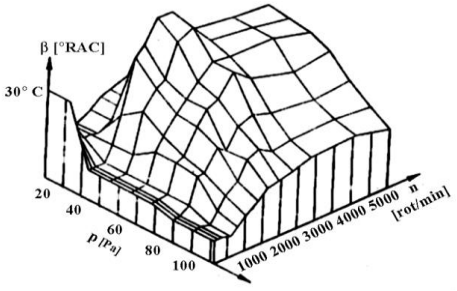

Figure 8 Renix multipoint system ignition mapping

Figure 9 shows the principle diagram of the Renix multipoint system that can be adapted to the Dacia Logan car.

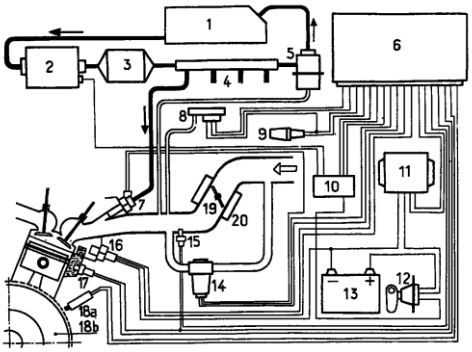

Figure 9 Principle diagram of the Renix multipoint system adapted on Dacia Logan: 1- fuel tank; 2- electric fuel pump; 3- fuel filter; 4- fuel distribution ramp at the injectors; 5- fuel pressure regulator; 6- computer; 7- injector; 8- absolute pressure transducer (air); 9- idle enrichment potentiometer; 10- control relay; 11- ignition power mode (MPI); 12- starting contactor; 13- battery; 14- electronic idle regulator; 15- air temperature transducer; 16- noise detector; 17- water temperature transducer; 18a- magnetic transducer (motor mode); 18b- solid sign of the flywheel; 19- flap; 20- box and flap contactor

They are proposed for determining the speed and the dead center of speed and angle reference transducers. They refer to the inductive transducer figure 10. [5] in which a magnetic field created by a permanent magnet 1 is partly wound on a steel core 2, is manifested in the air and in all neighboring media having a good magnetic conductivity. A gear wheel 3 with a steel pin 4 (reference mark) moving in front of the transducer changing the intensity and direction of the magnetic field. This variation of the magnetic field induces in the coil 5 an electric current of voltage U which is directed by the cable towards the electronic control unit.

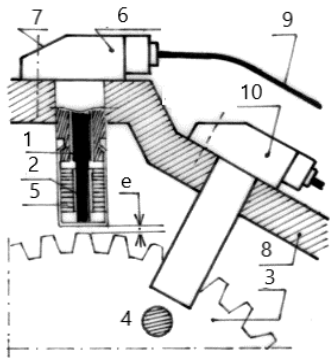

Figure 10 Speed and angular reference sensors: 1- permanent magnet; 2- steel core; 3- gear; 4- reference point; 5- coil; 6- speed sensor; 7- fixing device; 8- fixing support; 9- electric cable; 10- angular reference sensor; e - the interference between the crown and the sensor

The speed of the crankshaft is evaluated by an inductive speed transducer before which the teeth of the flywheel crown move. This transducer releases an output pulse on the tooth. The amplitude and shape of the electrical output signal transmitted by the computer depends on: the speed of rotation of the crown; the interference (e) between the crown and the sensor;

the profile of each tooth; the position (axial or radial) of the transducer in relation to the motor shaft; of the material in the sensor support.

The electronic control panel performs a signaling before being transmitted to the microcomputer. The angular position of the crankshaft is determined exactly by a position sensor or angular reference sensor which is also a pulse inductive sensor like the speed sensor. This sensor sends an output signal to the control panel with a pin or hole placed in front of it. There is an electrical output pulse for a crankshaft rotation. Without the crankshaft signal the engine does not start. For starting the minimum electric current is higher than 0.3 V. Resistance variation is 680 – 1200 Ω. When the speed signal is interrupted, the operation of the pump is cut off, the sensor performs the speed correction according to the speed. The sensor emits signals to synchronize the ignition with the injection. When oversaturated, it shuts off the injector.

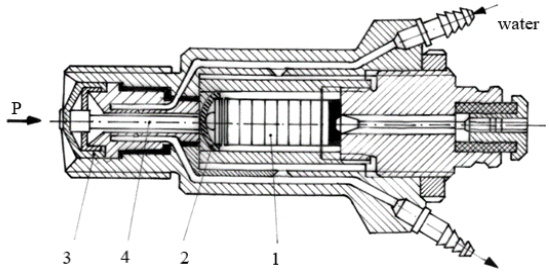

Figure 11 Piezoelectric pressure sensor

The diagram of the connection of the sensor in the measuring installation is shown in figure 12. The piezoelectric sensor imposes a typical structure of the adapter and auxiliary elements. The specific element of the adapter is the preamplifier PA, which has the role of adapting the high value output impedance of the sensor into one convenient for measurement and analysis. Obviously, this also amplifies the signal provided by the sensor. After preamplification, the signal passes through the I integrators, necessary to obtain signals proportional to the speed or displacement corresponding to the acceleration sensed by the sensor. The structure of the installation is completed with the module of the AM measuring amplifier, the block that provides the effective value BVE, and the filter block BF, which selects certain frequency ranges for the subsequent processing of the signal until the output.

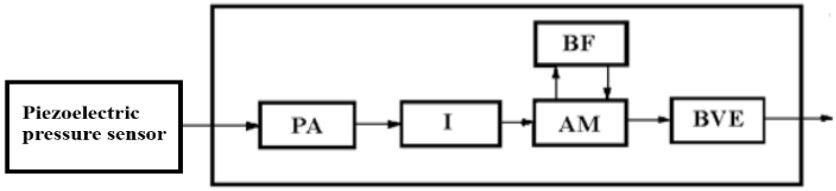

Figure 12 Sensor connection diagram in the measuring installation

6. THE REAL INDICATOR DIAGRAM

The general configuration of a test bed for the measurement of the parameters of a S.I. engine:

- The test bed on which the experimental data were acquired is provided with an electric machine with eddy currents of a W130 Shenk type.
- The setup of the test bed is presented in figure 13 [5].

Figure 13 The test bed used to obtain the indicator diagram

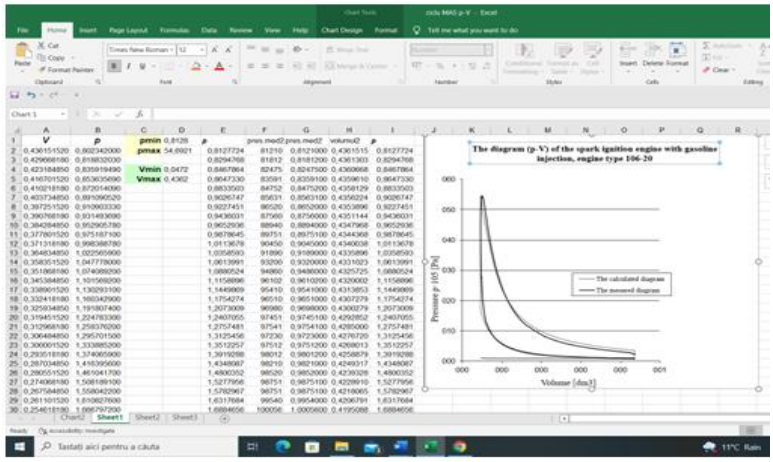

Figure 14 The capture with p-V cycle, the calculated and the measured chart the overlap

Specifications				
Measuring range			0...300 bar	
Overload			350 bar	
Lifetime	≥		10^8	load cycles
Sensitivity			19 pC/bar	nominal
Linearity	≤	±	0.3%	FSO
Natural frequency	~		170 kHz	
Acceleration sensitivity	≤		0.0005 bar/g	axial
Shock resistance	≥		2000 g	
Insulation resistance	≥		10^{13} Ω	at 20 °C
Capacitance			7.5 pF	
Operating temperature range			-40 ... 400 °C	
Thermal sensitivity change	≤		2 %	20 ... 400 °C
	≤	±	0.5 %	250 ± 100 °C
Load change drift			1.5 mbar/ms	max. gradient
Cyclic temperature drift *	≤	±	0.7 bar	
Thermo shock error **				
Δp	≤	±	0.4 bar	
Δp_{mi}	≤	±	2 %	
Δp_{max}	≤	±	1.5 %	
Thread diameter			M5x0.5	front sealed
Cable connection			M4x0.35	negative
Weight			2.2 grams	without cable
Mounting torque			1.5 Nm	

*) at 7 bar IMEP and 1300 rpm, diesel
**) at 9 bar IMEP and 1500 rpm, gasoline

Figure 15 The pressure sensor used for tests and its characteristics [5]

This numerical results for the cycle proposed by the author of Engines with Spark Lightning in corresponding conditions above it return in table 2 and figure 16.

Table 2 *The pressures and the rotation angle in the characteristic points of the engine cycle*

The point	The pressure (10^5 Pa)	The rotation angle [dgr]
r	1,13	0
r_1	0,8023	22
a	0,8023	180
c	16,4727	333
z	53,9902	365
u	37,9328	410
d	3,5918	537
d_1	1,13	540

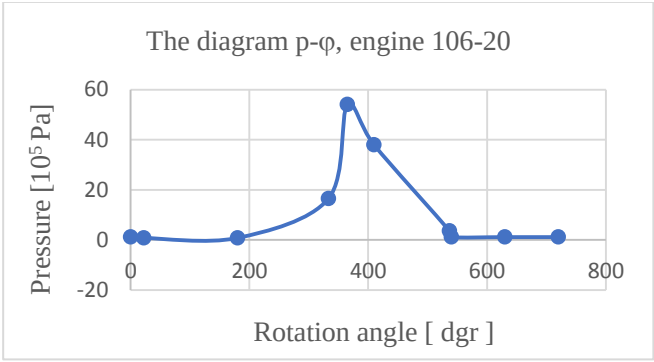

Figure 16 The diagram p-φ of cycle for Engines with Spark Lightning, whit gasoline injection, engine type 106-20

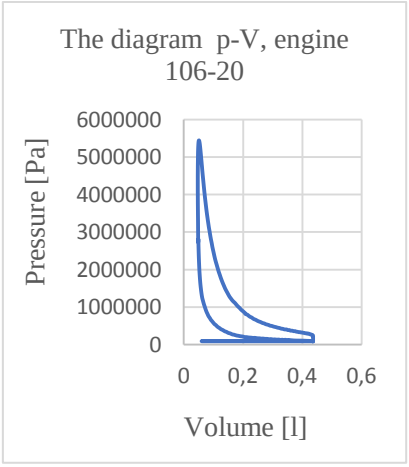

Figure 17 The measured diagram p-V

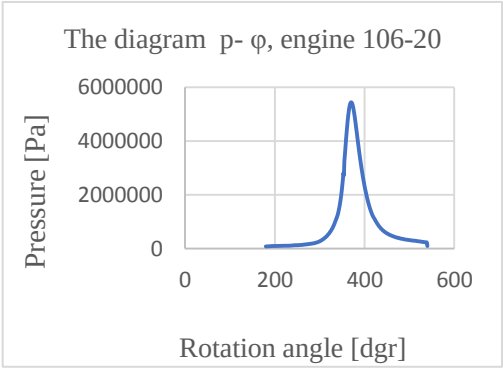

Figure 18 The measured diagram p-φ

7. CONCLUSIONS

The modelling of the SI engine cycle proposed by the authors consists in the presentation of the initial data of the computing program, the calculation and the correlation between the parameters of the engine for the realization of computing programs. The proposed model is a helping cycle to simulate the gasoline injection. The computer simulation permits the determination of the theoretical technical-economical parameters: the mechanical work corresponding to the rounded diagram, the indicated mean pressure, the indicated efficiency and the indicated specific fuel consumption. [1], [4]. After the calculation of the mechanical and the pumping losses, one can calculate the engine's effective technical-economical parameters. Using the model proposed in this paper, one can calculate the fuel mass injected per cycle, depending on the rotational speed at total load, the fuel flow through the electronic injector, reaching the purpose pursued, the determination of the injection duration depending on the rotational speed, at total load. It can be seen that the differences between the two data sets are in the range of 0.1-3.5%.

The calculated value of the pressure at the end of the intake process is 0.1% higher than the measured one. The pressure measured at the end of the compression stroke is 0.1% lower than the calculated one.

This small difference is due to the fact that the proposed model is almost similar to reality, and the pressure increase is higher than in the non-combustion cycle. However, the pressure difference at this point is small, because in this part (until the end of the compression stroke) only small amounts of fuel burn and, therefore, there is no significant amount of heat released.

Regarding the difference between the measured and the calculated value of the pressure at the end isochoric combustion, this is only 0.2%. However, the measured value is lower than the calculated one.

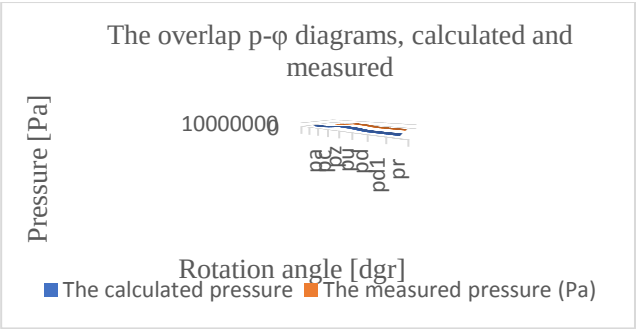

Figure 19 The overlap of the calculated and the measured indicator diagram p-φ

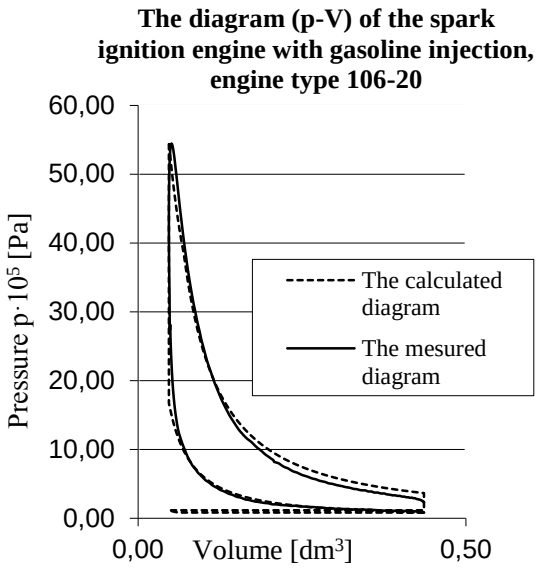

Figure 20 The overlap of the calculated and the measured indicator diagram p-V

Table 3 *The error betwenn the calculated and measured values in the characteristic points of the engine cycle*

The point	The calculated pressure [Pa]	The measured pressure [Pa]	The error [%]
a	81272	81210	0,1%
c	1668684	1667088	0,1%
z	5469207	5462756	0,2%
u	3842592	3841275	0,1%
d	363849	358818	1,4%
d1	114469	110466	3,5%
r	114469	110466	3,5%
r1	81272	81210	0.1%

At the end of post-combustion, the measurement is 0.1% lower than the calculated one. This can be explained by the fact that since the assumption that the combustion process begins in TDC, in theoretically the amount of fuel burned in the isochoric phase is less than the actual one. So, in the post-combustion, in the theoretical cycle, a smaller amount of fuel remains to be burned [4]. On the other hand, at the end of the expansion stroke, the measured value of the pressure is 3.5% lower than the calculated one, being the biggest difference, which is also visible on the overlapping diagrams. The difference in the exhaust pressure is also a maximum of 3.5%. This is probably the difference because the pressure is not measured in this region, but is estimated based on the minimum, maximum and average pressures at the characteristic points of the cycle. The values of the temperatures calculated at the characteristic points of the engine cycle were according to the statistical data. It was noticed that the calculated values are inside recommended intervals. If it is possible to develop a model for the study of ICE operation at low or medium load levels, it will be possible to

determine the parameters that ensure a minimum fuel consumption and pollutant emissions at a certain operating regime. So, the model proposed in this paper, which proved to have a very good accuracy (and this can be improved) can be used to study the operation of SI motors in different conditions.

The program was used to study other normally aspirated SI gasoline injection engines.

The most conclusive gain for the Dacia Logan's petrol injection engine is the depollution of the engine. The pollutant emissions tests carried out in the Bosch laboratories at Schwieberdinger (under the control of UTAC-France representatives as the approval authority) have already confirmed that Dacia Logan complies with the depollution rules in force. The Renix multi-point injection system, which equips Renault engines with 4 cylinder Dacia cars, has been adapted to increase engine performance, reduce engine size, reduce fuel consumption, reduce fuel consumption and reduce pollution. Experienced petrol injection engines are superior to carburetor engines by reducing fuel consumption and pollutant emissions as well as dynamic construction and operating performance. The authors also intend to use this model for turbo engines.

REFERENCES

[1] Blaga, V.: "Engines with Gasoline Injection", Oradea: University of Oradea Publishing House, 2013, ISBN-978-606-10-1004-2.

[2] Blaga, V., Mitran, T., Moca, S., Chioreanu, C.: "The calculus of the pressures in the characteristic points of the engine'cycle for a DGI engine", The 30th SIAR International Congress of Automotive and Transport Engineering Science and Management of Automotive and Transportation Engineering, Craiova, 2017, ISBN 978-3-030-32563-3, pp. 3-14.

[3] Blaga, V., Mitran, T., Dragomir, G., Fagadar, D.: "The calculus of the temperatures in the characteristic points of the gasoline direct injection engine cycle", Annals of the University of Oradea, Fascicle of Management and Technological Engineering, Oradea, May, 2019, ISSN 2501-5797.

[4] Blaga, V.: "Processes and Characteristics of the Internal Combustion Engines", University of Oradea Publishing House, Oradea, 2013.

[5] Blaga, V., Mitran, T., Rus, A., Beles, H., Dragomir, G.: "A comparative study of calculated and experimental indicator diagrams of a S.I. Engine AITS 2021", IOP Conf. Series: Materials Science and Engineering; 1220 (2022) 012016.G, 2021.

[6] Mitran, T., Blaga, V., Beles, H., Dragomir, G.: "The calculus of the technical-economic parameters a spark–ignited direct injection engine", Revista SIAR, No. 48, September, 2018.

[7] Mitran, T., Blaga, V., Moca, S.: "The Calculation Algorithm for the Determination of the Intake Stroke for GDI Engines", Engines Brasov: International Congress of Automotive and Transport Engineering, 2017, pp. 311-318.

MOBILITY & VEHICLE MECHANICS

https://doi.org/10.24874/mvm.2022.48.03.02
UDC: 621.43.053

THE ANALYSIS OF THE UNCONVENTIONAL PISTON MECHANISM CONCEPTION AND COMPARISON WITH THE CONVENTIONAL PISTON MECHANISM

*Ivan Grujić [1], Sunny Narayan [2], Nadica Stojanović [3]**

Received in August 2022 *Revised in September 2022* *Accepted in October 2022*

RESEARCH ARTICLE

ABSTRACT: The IC engines construction is usually neglected by the engineers, so because of this, the last few decades cannot notice big changes from the aspect of the construction of engine mechanical parts. The greatest accent was given to the reduction of the exhaust emission, and with this on the IC engines equipment improvement. In the paper was conducted the analysis of the unconventional piston mechanism, as well as the comparison with classic/conventional piston mechanism. Results show a many advantages from the aspect of IC engine construction, reliability, working cycle and performances, which can be achieved with IC engine with this piston mechanism, and small number of disadvantages, which easy can overcome.

KEY WORDS: *IC engine, unconventional piston mechanism, construction, reliability*

[1]*Ivan Grujic, University of Kragujevac, Faculty of Engineering, Sestre Janjic 6, 34000 Kragujevac, Serbia, ivan.grujic@kg.ac.rs,* ORCID ID: 0000-0003-0572-1205
[2]*Sunny Narayan, Qassim university, 52571 Qassim Region, Mechanical engineering department, Saudi Arabia, rarekv@gmail.com,* ORCID ID: 0000-0001-7033-6341
[3]*Nadica Stojanovic, University of Kragujevac, Faculty of Engineering, Sestre Janjic 6, 34000 Kragujevac, Serbia, nadica.stojanovic@kg.ac.rs,* ORCID ID: 0000-0002-4199-0587 *(*Corresponding author)*

ANALIZA NEKONVENCIONALNE KONCEPCIJE KLIPNOG MEHANIZMA I UPOREĐIVANJE SA KONVENCIONALNIM KLIPNIM MEHANIZMOM

REZIME: Konstrukcija motora SUS uglavnom je zapostavljena od strane inženjera, te samim tim poslednjih nekoliko decenija ne mogu se uočiti velike promene sa aspekta konstrukcije mehaničkih delova motora. Najveći akcenat je bačen na smanjenje izduvne emisije, te samim tim na usavršavanje opreme motora. U radu je izvršena analiza nekonvencionalne konstrukcije klipnog mehanizma i upoređivanje sa klasičnim konvencionalnim klipnim mehanizmom. Rezultati pokazuju niz pogodnosti sa aspekta konstrukcije, pouzdanosti, radnog ciklusa i performansi, koje se mogu postići ukoliko bi se razmišljalo o proizvodnji motora sa ovakvim klipnim mehanizmom, uz veoma mali broj nedostataka koji se lako mogu prevazići.

KLJUČNE REČI: *motor SUS, nekonvencionalni klipni mehanizam, konstrukcija, pouzdanost*

THE ANALYSIS OF THE UNCONVENTIONAL PISTON MECHANISM CONCEPTION AND COMPARISON WITH THE CONVENTIONAL PISTON MECHANISM

Ivan Grujić, Sunny Narayan, Nadica Stojanović

INTRODUCTION

IC engines by decades represent an irreplaceable type of drive train for almost all mobile systems. Nevertheless, over a past few years is discussing about the ecology and harmful effect of IC engines, so due this, is predicting their replacement with electric drive train, however, it doesn't exist clear image will be IC engine ever be replaced or not. All these predictions are related with the exhaust emission which cannot be avoided in the case of IC engines. However, the replacement of IC engines with the electric drive train doesn't mean suppression of exhaust emission, but only it dislocation. Also the introduction of a full vehicles electrification demands infrastructure and material resources, for which raises a question, whether they exist. Because all mentioned, it is quite clear that the IC engines are the past, but also and the future of automotive, shipbuilding and other industries, and they will be used in decades which come [1].

From the day of the origin, until today, IC engines have experienced a great progress, from the aspect of performances, economy and exhaust emission. All this changes have become possible thanks to the technology progress, and by its application through systems on IC engines. Nevertheless, the basic construction of the IC engine piston mechanism from the day of the origin, until today have stayed pretty much similar. So because of this, maybe future researches should be directed to the improvement of IC engine piston mechanism, in order to make a new types of IC engines with better characteristics.

Today, standards which are related to the fuel consumption are more and more strict, so from the vehicles with IC engines is expect to have as better possible performances with minimal fuel consumption. One of the solutions which are today widely used at gasoline IC engines, in order to reduce the fuel consumption and by this the exhaust emission is gasoline injection direct to the cylinder, instead to the intake port [2]. Fuel consumption also can be reduced by application of different engine conception [3, 4].

Besides the fuel consumption also should consider the thermal stresses which appear in the engine, and to reduce them to the minimum, how was conducted in the research of Hu et al. [5] on the engine with opposed piston opposed cylinder. Besides that, by application of such engine its obtain the very convenient ratio of surface/volume, shorter combustion, smaller heat loses and more efficient cylinder cleaning [6-8], a besides all of this, was obtained a greater brake thermal efficiency compare to the same power four stroke diesel engine, as well as, lower emission [9, 10]. The exhaust emission can be reduced in many ways by construction parameters. For example, the emission of NOx, directly is related to the temperatures which appear in the engine cylinder, son on this can be affected by application of engine with variable compression ratio [11], as well as, by application of HCCI (homogeneous charge compression ignition) engines which give a low emission of nitric oxides, and besides this can achieve a great efficiency [12]. High-pressure direct injection (HPDI) at diesel Wankel engine reduces the particle emission for 39.5% [13]. Besides using the specific engine constructions, and modern engine equipment, the emission of diesel engine can be reduced and by addition biodiesel [14]. Application of the Achates Power opposed-piston, two-stroke diesel engine provides better reliability and low fuel

consumption, which makes this conception good for application at commercial vehicles in the future.

One more important thing for IC engine, besides its emission, are its performances. Always is tend to develop such IC engine, which will have a good performances. So because of this are developed some unconventional engines, which performances were compared to the performances of convention engines. One type of unconventional engine which was developed and tested is the crank-rocker engine. By application of the crank-rocker engine, it achieves 6.28% greater torque and power compare to the conventional slider-crank engine [15]. Other variant of engine with which are achieving better performances compare to the conventional engine is the Duke engine [16].

The main aim of this paper is kinematic-dynamic analysis of unconventional piston mechanism and comparison with the conventional piston mechanism, in order to represent the potential advantages and disadvantages of analysed solution.

1. UNCONVENTIONAL PISTON MECHANISM

Related to the construction and kinematic characteristics, the existing, more or less used piston mechanisms, can be divided on two types and that:

- Piston mechanism with translational piston movement and
- Piston mechanism with the rotational piston movement.

For the piston mechanism with the translational piston movement freely can be said that this piston mechanism is the classic piston mechanism which is present in almost all IC engines, different from this piston mechanism, engine with piston mechanism with the rotational piston movement, widely known as Wankel engine, represents an engine with quite different piston mechanism. The greatest advantage of engines with the rotational piston movement compare to the mechanism with the translational piston movement is the smaller number of moving parts, as well as the great power for smaller engine displacement. Nevertheless, the disadvantages pf this type of engines, which are the consequence of the engine construction are next:

- Difficult engine sealing,
- Uneven thermal stresses,
- Faster wear and
- Relatively short life cycle.

In order to take advantages and to remove the disadvantages of both types of engines, sometimes the most obvious solution is to make the combination of both of them. Therefore, the analysed type of piston mechanism, in some way can be considered as the combination of the piston mechanism with translational piston movement and piston mechanism with rotational piston movement, Figure 1.

The created model from the Figure 1 corresponds to piston mechanism of a six cylinder engine with the displacement of 2977 cm^3, that is, 3.0 L engine. Of course, the same principle can be applied and for engines with less or more cylinders. The application of translational piston movement provides good sealing between the cylinder block and cylinder head, which is characteristic for the engines with the translational piston movement. Different from that, the application of gears instead the connecting rods, as at the Wankel engine, provides the reduction of the entire engine dimensions as well as engine

mass. Further the mass reduction will positively affect on the fuel consumption reduction and by that on the exhaust emission reduction.

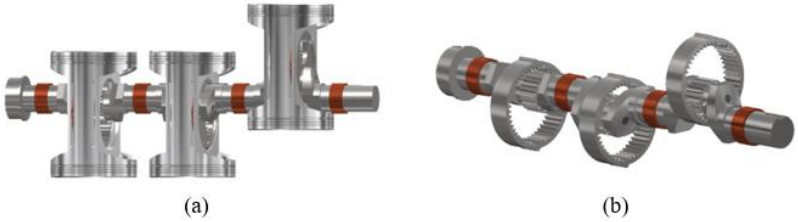

Figure 1 3D model of (a) analysed unconventional piston mechanism and (b) connection between the crankshaft and pistons

2. KINEMATIC-DYNAMIC ANALYSIS AND COMPARISON

How the main difference between conventional and unconventional piston mechanism is in construction, main differences which lead to the advantages or disadvantages should look for in the kinematic and dynamic characteristics, which further have influence on the engine work. Kinematic schemes of conventional and unconventional piston mechanism on basis of which can be determined kinematic characteristics are given on the Figure 2.

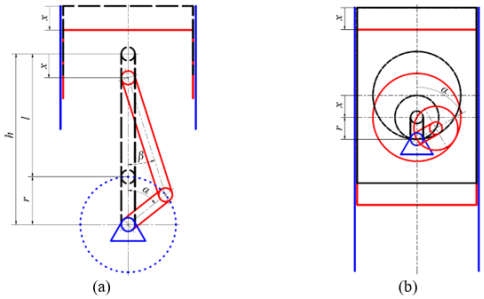

Figure 2 Kinematic scheme of (a) conventional piston mechanism and (b) unconventional piston mechanism

The kinematic characteristics of both mechanism can be simply determined by application of the trigonometric equations and functions. Kinematic characteristics determined in this paper for both types of mechanism are piston path, piston speed and piston acceleration. The equations for listed characteristics are next:

- piston path for the conventional piston mechanism

$$x = h - r \cdot \cos\alpha - l \cdot \cos\beta \tag{1}$$

where is:

$$\beta = \arcsin\left(\frac{r \cdot \cos\alpha}{l}\right) \tag{2}$$

- piston path for the unconventional piston mechanism

$$: x = 2 \cdot r - 2 \cdot r \cdot \cos\alpha \tag{3}$$

- piston speed for the conventional piston mechanism

$$v = \frac{dx}{dt} \cdot \frac{d\alpha}{d\alpha} = \omega \cdot \frac{dx}{d\alpha} = \omega \cdot \left(r \cdot \sin\alpha + l \cdot \frac{d\beta}{d\alpha} \cdot \sin\beta \right) \tag{4}$$

- piston speed for the unconventional piston mechanism

$$v = \frac{dx}{dt} \cdot \frac{d\alpha}{d\alpha} = \omega \cdot \frac{dx}{d\alpha} = 2 \cdot \omega \cdot r \cdot \sin\alpha \tag{5}$$

- piston acceleration for the conventional piston mechanism

$$a = \frac{dv}{dt} \cdot \frac{d\alpha}{d\alpha} = \omega \cdot \frac{dv}{d\alpha} = \omega^2 \cdot \left(r \cdot \cos\alpha + l \cdot \frac{d^2\beta}{d\alpha^2} \cdot \sin\beta + l \cdot \left(\frac{d\beta}{d\alpha} \right)^2 \cdot \cos\beta \right) \tag{6}$$

- piston acceleration for the unconventional piston mechanism

$$a = \frac{dv}{dt} \cdot \frac{d\alpha}{d\alpha} = \omega \cdot \frac{dv}{d\alpha} = 2 \cdot \omega^2 \cdot r \cdot \cos\alpha \tag{7}$$

By analysis of equations from (1) to (7), can be noticed that the equations for the kinematic characteristics of the unconventional piston mechanism are much more simple compare to the equations for the determination of kinematic characteristics of conventional piston mechanism. Even more, for the determination of the piston acceleration, in the case of the unconventional piston mechanism, it is not necessary to use nonlinear differential equation as in the case for the conventional piston mechanism. Differences in the equations lead to conclusion that are existing differences in kinematic characteristics. For better understanding, what main differences are, it was performed the determination of kinematic characteristics for conventional and unconventional piston mechanism with the same geometrical characteristics of engine (cylinder bore and piston stroke), Figures 3 to 5.

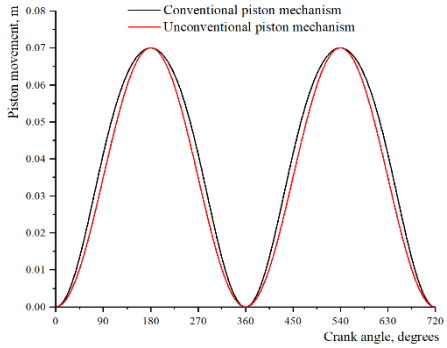

Figure 3 Piston path

By analysing diagram from Figure 3, it can be seen that exist a noticeable difference in the piston path of the conventional an unconventional piston mechanism. The most important difference that can be crucial for the engine work is the piston path behaviour in the area of TDC (Top Dead Centre). In the case of unconventional piston mechanism, piston stays a little bit longer in the area of TDC, which means that the combustion will happen in the conditions which are more similar to the combustion at constant volume. This means that unconventional piston mechanism can approach the engine working cycle to the ideal Otto cycle and in this way to increase the efficiency.

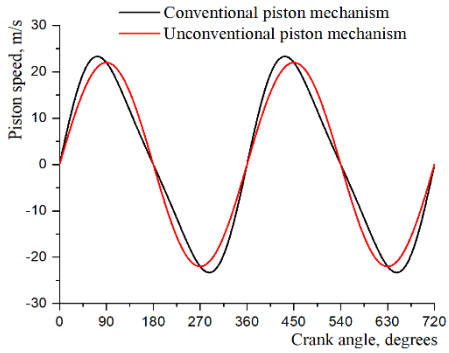

Figure 4 Piston speed

Logically, the differences in the piston path have caused the differences in the piston speed. In the case of the unconventional piston mechanism, the piston speed can be described by sine function which depends only from the crankshaft angle, while in the case of the case of conventional piston mechanism, piston speed depends and from the position angle of the connecting rod. However, the piston speed is not interest from the aspect of engine work. More interesting is the piston acceleration, which is given on the Figure 5.

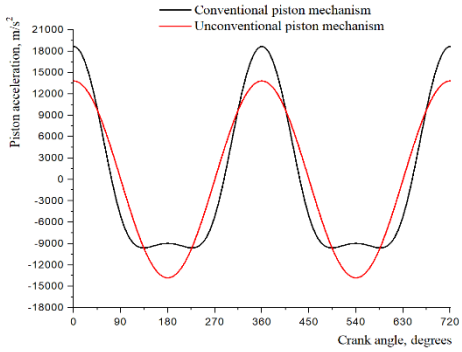

Figure 5 Piston acceleration

Piston acceleration is quite important, because directly influences on the inertial force which acts on the piston. Also, a good know fact is that acceleration is directly related to the vibrations and instability. By observing accelerations curves from Figure 5, it can be seen that the piston acceleration of unconventional piston mechanism corresponds to cosine function, which confirms and equation (7). However in the case of the conventional piston mechanism, the piston acceleration is described by nonlinear differential function. All these difference are appearing exactly because conventional piston mechanism has and unconventional piston mechanism doesn't have the connecting rod. According to the shape of the piston acceleration curves, it can be said that the engine with unconventional piston mechanism will have more stable work.

Further analysis and comparison of conventional and unconventional piston mechanism is based on the dynamic of the piston mechanism, that is, on forces which act inside the piston mechanism during the engine work. Dynamic schemes which were used for determination of dynamic characteristics are given on Figure 6.

For detail dynamic analysis, it is necessary to know the values of the cylinder pressure for the entire working cycle. Therefore, how the unconventional piston mechanism is not made

yet, in continues will be conducted only an analytical analysis, on the basis of the equations which describe the forces from Figure 6.

The gas force which is directly related to the cylinder pressure, in both cases, and for conventional and for unconventional piston mechanism, can be calculated by the same equation, equation (8):

$$F_g = \frac{D^2 \cdot \pi}{4} \cdot \left(p_g - p_0 \right) \tag{8}$$

where are:

- p_g – cylinder pressure,
- p_0 - pressure in the crankcase under the piston (approximately equal to the environment pressure).

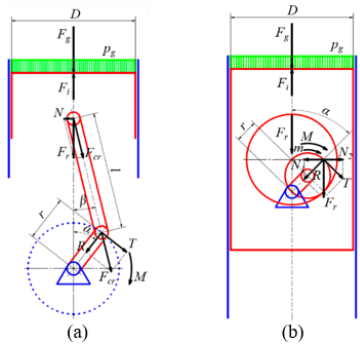

Figure 6 Dynamic scheme of (a) conventional piston mechanism and (b) unconventional piston mechanism

In both cases can be used the same equation for calculation of the gas force. However, on the gas force, the greatest influence has the cylinder pressure, which means that the gas force will have the greatest value in the area of TDC. If take into consideration, previous said that the cylinder pressure will be affected due to the different piston path (piston stays longer in the area of TDC in the case of unconventional piston mechanism and this influences on the combustion process), it can conclude that the gas force will surely be different for unconventional in respect to the conventional piston mechanism.

Inertial force also ca be calculated with the same equation for both piston mechanisms, conventional and unconventional, equation (9):

$$F_i = m \cdot a \tag{9}$$

where are:

- m – mass of the piston group and
- a - piston acceleration.

As in the case of the gas force, also in this case, the same equation doesn't mean that the values of the inertial force will be the same. First of all the piston acceleration in the case of the unconventional piston mechanism is quite different than the piston acceleration of the conventional piston mechanism. Also the value of the acceleration in the area of the TDC in the case of the unconventional piston mechanism is less than in the case of the conventional piston mechanism which will lead to the greater resulting force (equation (10)) in this area. Also second parameter which influences on the inertial force is the mass of the piston group which in the case of the conventional piston mechanism consists from masses of: piston,

piston rings, wrist pin, snap rings (if they are exist) and one part of the connecting rod mass, while in the case of unconventional piston mechanism, mass of the piston group consists from: piston, piston rings, piston cap, piston gear, piston bearing, snap ring. So all told leads to the conclusion that surely will exist differences in the values of the inertial force.

$$F_r = \pm F_g \pm F_i \tag{10}$$

The force which doesn't exist in the case of the unconventional piston mechanism is the connecting rod force, which in the case of the conventional piston mechanism can be calculated by the equation (11).

$$F_{cr} = \frac{F_r}{\cos\beta} \tag{11}$$

The greatest mechanical advantage of the unconventional piston mechanism is because it doesn't have a connecting rod. Thanks to this in the case of the unconventional piston mechanism doesn't exist normal force, which in the case of the conventional piston mechanism can be calculated by equation (12).

$$N = F_r \cdot tg\beta \tag{12}$$

Normal force is undesirable force which pushes piston along the cylinder wall. This causes friction force between piston and the cylinder, which eventually leads to the wear and the engine failure. Different than the conventional piston mechanism, in the case of unconventional piston mechanism are appearing two normal forces, shown on Figure 7.

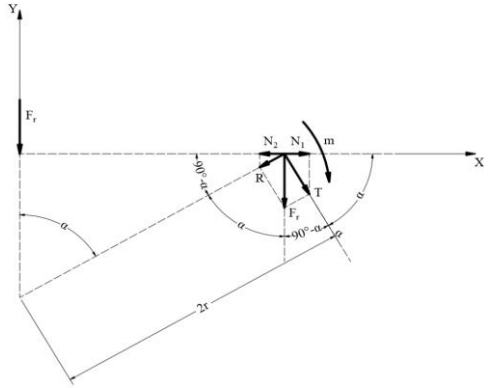

Figure 7 Forces

For the calculation of normal forces which appear in the case of the unconventional piston mechanism, it is necessary to know the values of tangential force and radial force, which can be calculated by equations (13) and (14).

$$T = F_r \cdot \sin\alpha \tag{13}$$

$$R = F_r \cdot \cos\alpha \tag{14}$$

While in the case of the conventional piston mechanism, tangential force and radial force can be calculated by equations (15) and (16).

$$T = F_{cr} \cdot \cos\left(90° - \left(\alpha + \beta\right)\right) \tag{15}$$

$$R = F_{cr} \cdot \sin\left(90° - \left(\alpha + \beta\right)\right) \tag{16}$$

So according to the Figures 6 and 7, and equations (13) and (14), the equations for the calculation of normal force for the unconventional piston mechanism are next:

$$N_1 = T \cdot \cos\alpha = F_r \cdot \sin\alpha \cdot \cos\alpha \tag{17}$$

$$N_2 = R \cdot \cos(90° - \alpha) = F_r \cdot \cos\alpha \cdot \cos(90° - \alpha) = F_r \cdot \sin\alpha \cdot \cos\alpha \tag{18}$$

By analysis of relations (17) and (18), it can be seen that the normal forces have the same value, and from Figures 6 and 7 can be seen that this forces have opposite direction, which means that the one will suppress another, that is, in the case of the unconventional piston mechanism, the normal force which push the piston along the wall of the cylinder doesn't exist. This leads to the conclusion that is real to expect a longer life cycle from the engine with unconventional piston mechanism, as well as better mechanical efficiency.

At the end, one more advantage of the unconventional piston mechanism, can be found in better performances of the engine. This can be proved by comparing the equations for torque for conventional (19) and unconventional piston mechanism (20).

$$M = T \cdot r \tag{19}$$

$$M = T \cdot 2 \cdot r + F_r \cdot 2 \cdot r \cdot \sin\alpha = T \cdot 2 \cdot r + m \tag{20}$$

By analysing equations (19) and (20), it can be seen that in the case of the unconventional piston mechanism, torque is equal to the sum of two torques, where one comes from the tangential force as in the case of conventional piston mechanism, and other appears due the translation of resulting force, which means that engine with unconventional piston mechanism easy can have a greater torque and by that and greater power than the engine with the conventional piston mechanism.

3. CONCLUSIONS

In the paper was conducted analytical analysis of the unconventional piston mechanism and comparison with the conventional piston mechanism. The unconventional piston mechanism analysed in the paper represents the combination of the piston mechanism with translational piston movement and piston mechanism with rotational piston movement. By analysis of: geometrical, kinematic and dynamic characteristics, it can conclude, that the unconventional piston mechanism provides a many advantages compare to the conventional piston mechanism such are: smaller dimensions and by that less mass of the entire engine, combustion at almost constant volume, more stable work, nonexistence of normal force (wear reduction and by that increment of the reliability and life cycle), and compare to the classic rotational engines, unconventional piston mechanism provides better sealing, more even thermal stresses. All these advantages lead to the conclusion that this type of engine is maybe ideal for implementation in branches where a high reliability is necessary, for example military industry or shipbuilding industry. Also should not forget and the fact that this type of piston engine can lead to a possibility to obtain greater power for the same displacement of engine with the conventional piston mechanism. However, the main disadvantage is relatively complex construction, and because of this probably a greater

price. However in the braches such are military and shipbuilding industry these disadvantage should not be an obstacles. How all claims are based on the analytical analysis, it should made a many more researches related to the analysed piston mechanism. In future it is necessary to calculate and analyse the loads of the gear couple. This demands a concrete values of forces, which means that is necessary to know the values of the cylinder pressure. So the next step should be to made a model of working cycle of IC engine with unconventional piston mechanism, for example in some specialized software, in order to obtain the values of the cylinder pressure, and in the case of encouraging results, the next step will be the construction and manufacturing of engine prototype which will be tested.

ACKNOWLEDGMENTS

This paper was realized within the framework of the project "The research of vehicle safety as part of a cybernetic system: Driver-Vehicle-Environment", ref. no. TR35041, funded by the Ministry of Education, Science and Technological Development of the Republic of Serbia.

REFERENCES

[1] Naber, J., Johnson, J.: "Internal combustion engine cycles and concepts", in Folkson, R. (Ed.): Alternative Fuels and Advanced Vehicle Technologies for Improved Environmental Performance, 2014, pp. 197-224.

[2] Pawlak, G.M., Wołczyński, Z.: "The indicator of GDI engine operating mode and its influence on eco-driving", Applied Sciences, 2022, Vol. 12, No. 5, p. 2325, doi: 10.3390/app12052325.

[3] Kalke, J., Opaliński, M., Szczeciński, M.: Opposed-piston engines: the future of internal combustion engines?, in Czubenko, M. (Ed.) PhD Interdisciplinary Journal, 2014, pp. 175-184.

[4] Kooverjee, N.: Revolutionary 25,000-rpm engine is the next step of internal combustion, 2022, available at: https://carbuzz.com/news/revolutionary-25000-rpm-engine-is-the-next-step-of-internal-combustion, accessed: 18.10.2022.

[5] Hu, X., Sun, Q., Li, G., Ba, S.: "Numerical investigation of thermo-hydraulic performance of an opposed piston opposed cylinder engine water jacket with helical fins", Applied Thermal Engineering, 2019, Vol. 159, p. 113824, doi: 10.1016/j.applthermaleng.2019.113824.

[6] Regner, G., Fromm, L., Johnson, D., Koszewnik, J., Dion, E., Redon, F.: "Modernizing the opposed-piston, two-stroke enginefor clean, efficient transportation", SAE Technical Paper, 2013, 2013-26-0114, doi: 10.4271/2013-26-0114.

[7] Liu, Y., Zhang, F., Zhao, Z., Cui, T., Zuo, Z., Zhang, S.: "The effects of pressure difference on opposed piston two stroke diesel engine scavenging process", Energy Procedia, 2017, Vol. 142, pp. 1172-1178, doi: 10.1016/j.egypro.2017.12.374.

[8] Yang, W., Li, X.R., Kang, Y., Zuo, H., Liu, F.S.: "Evaluating the scavenging process by the scavenging curve of an opposed-piston, two-stroke (OP2S) diesel engine", Applied Thermal Engineering, 2019, Vol. 147, pp. 336-346, doi: 10.1016/j.applthermaleng.2018.10.095.

[9] Johnson, D., Koszewnik, J., Fromm, L., Redon, F., Regner, G.: "Opposed-piston, two-stroke diesel engine advantages in meeting higher fuel efficiency and emissions

standards", In 3rd Aachen Colloquium China Automobile and Engine Technology, 17-18 November, 2013, pp. 1-20.

[10] Mattarelli, E., Cantore, G., Rinaldini, C.A., Savioli, T.: "Combustion system development of an opposed piston 2-stroke diesel engine", Energy Procedia, 2017, Vol. 126, pp. 1003-1010, doi: 10.1016/j.egypro.2017.08.268.

[11] Shaik, A., Moorthi, N., Rudramoorty, R.: "Variable compression ratio engine: a future power plant for automobiles – an overview", Proceedings of the Institution of Mechanical Engineers, Part D: Journal of Automobile Engineering, 2007, Vol. 221, pp. 1159-1168, doi: 10.1243/09544070JAUTO573.

[12] Jamsran, N., Park, H., Lee, J., Oh, S., Kim, C., Lee, Y., Kang, K.: "Influence of syngas composition on combustion and emissions in a homogeneous charge compression ignition engine", Fuel, 2021, Vol. 306, p. 121774, doi: 10.1016/j.fuel.2021.121774.

[13] Chen, W., Yu, S., Pan, J., Fan, B., Zuo, Q., Zhang, B., Zhu, G., Yang, X.: "Effect analysis of the forward flow fuel injection angle on stratified combustion process in a high-pressure direct injection diesel Wankel engine (HPDI-DWE)", Energy Conversion and Management, 2022, Vol. 253, p. 115179, doi: 10.1016/j.enconman.2021.115179.

[14] Yeom, J.K., Yoon, J.H.: "A proposal of quantitative analysis method of emission characteristics of biodiesel fuel in diesel engine", International Journal of Precision Engineering and Manufacturing, 2015, Vol. 16, pp. 1269-1277, doi: 10.1007/s12541-015-0166-2.

[15] Mohammed, S.E., Baharom, M.B., Aziz, A.R.A.: "Performance and combustion characteristics of a novel crank-rocker engine", Journal of Mechanical Science and Technology, 2017, Vol. 31, pp. 3563-3571, doi: 10.1007/s12206-017-0643-x.

[16] Joshi, S.: "Duke Engine: An overview of present state of art and future potential", International Journal of Scientific Engineering and Research (IJSER), 2016, Vol. 4, pp. 15-18.

MOBILITY & VEHICLE MECHANICS

https://doi.org/10.24874/mvm.2022.48.03.03
UDC: 629.3.016.8

DEVELOPMENT OF THE MODERN AUTOMOTIVE INDUSTRY BASED ON THE SOLAR TECHNOLOGY APPLICATION

Natalija Aleksić [1], Danijela Nikolić [2], Vanja Šušteršič [3], Saša Jovanović [4]*

Received in September 2022 *Accepted in November 2022*

RESEARCH ARTICLE

ABSTRACT: In the past decades, the automotive industry is growing proportionally with the rapid population increase. On the other hand, increasing energy consumption and the use of fossil fuels have led to increased environmental pollution. A new trend in the automotive industry in the last twenty years is the development of new types of vehicles that are powered by renewable energy and the solar-powered vehicle is very popular among them. Solar photovoltaic technologies are very convenient for electric and hybrid vehicles, due to the direct conversion of solar energy to electricity, the low cost of photovoltaic panels, and their positive environmental impact. There are various types of solar cars developed by different companies, which have remarkable development in terms of materials, energy management systems, and used mechanical and electrical components. This paper represents an overview of solar energy applications in the automotive industry and the development of solar and hybrid cars. Also, a comparative analysis of different solar vehicles is presented, with the possibilities for further investigation and development of solar energy applications in the automotive industry.

KEY WORDS: *automotive industry, photovoltaics, solar vehicle, hybrid solar vehicle*

[1] *Natalija Aleksić, University of Kragujevac, Faculty of Engineering, Sestre Janjić 6, 34000 Kragujevac, Serbia, natalija94u@gmail.com,* ORCID ID: - *(*Corresponding author)*
[2]*Danijela Nikolić, University of Kragujevac, Faculty of Engineering, Sestre Janjić 6, 34000 Kragujevac, Serbia, danijelan@kg.ac.rs,* ORCID ID: 0000-0003-3267-3974
[3]*Vanja Šušteršič, University of Kragujevac, Faculty of Engineering, Sestre Janjić 6, 34000 Kragujevac, Serbia, vanjas@kg.ac.rs,* ORCID ID: 0000-0001-7773-4991
[4] *Saša Jovanović, University of Kragujevac, Faculty of Engineering, Sestre Janjić 6, 34000 Kragujevac, Serbia, dviks@kg.ac.rs,* ORCID ID: 0000-0001-5916-2483

RAZVOJ MODERNE AUTOMOBILSKE INDUSTRIJE ZASNOVANE NA PRIMENI SOLARNE TEHNOLOGIJE

REZIME: Poslednjih decenija razvoj automobilske industrije je rastao proporcionalno sa naglim porastom stanovništva. S druge strane, povećana potrošnja energije i upotreba fosilnih goriva doveli su do povećanog zagađenja životne sredine. Novi trend u automobilskoj industriji u poslednjih dvadesetak godina je razvoj novih tipova vozila koja za pogon koriste obnovljivu energiju i među njima su veoma popoularna solarna vozila. Solarne fotonaponske tehnologije su veoma pogodne za električna i hibridna vozila, zbog direktne konverzije solarne energije u električnu energiju, niske cene fotonaponskih panela i njihovog pozitivnog uticaja na životnu sredinu. Postoje različiti tipovi solarnih automobila koje su razvile različite kompanije, koji imaju značajan razvoj u pogledu materijala, sistema upravljanja i korišćenih mehaničkih i električnih komponenti. Ovaj rad predstavlja pregled primene solarne energije u automobilskoj industriji i razvoj solarnih i hibridnih automobila. Takođe, prikazana je komparativna analiza različitih tipova solarnih vozila, sa mogućnostima daljeg razvoja primene solarne energije u automobilskoj industriji.

KLJUČNE REČI: *automobilska industrija, fotonaponski paneli, solarna vozila, hibridna solarna vozila*

DEVELOPMENT OF THE MODERN AUTOMOTIVE INDUSTRY BASED ON THE SOLAR TECHNOLOGY APPLICATION

Natalija Aleksić, Danijela Nikolić, Vanja Šušteršič, Saša Jovanović

INTRODUCTION

The idea of an electric vehicle has a history longer than 100 years. More than a decade ago, the search for the development of Zero-Emission Vehicles (ZEV), Electric Vehicles (EV), and Hybrid Electric Vehicles (HEV) [1-3] had taken a new influence. The interest in these vehicles has grown, mainly because of their characteristics that reduce pollution. Over the past 10 years, the significant development of electric and hybrid vehicles was noted. Also, over the last few years, there are more and more discussions about the development and production of solar cars and hybrid solar cars. Solar cars use solar energy by photovoltaicls, rechargeable batteries, and use that energy to power the vehicle's electric motor. However, to apply solar energy to vehicles, it is necessary to carefully analyse critical points, such as the efficiency and cost of photovoltaic panels, as well as to consider how to maximize solar radiation and how to manage and to control obtained energy [4, 5].
Today, there are three types of solar cars in the literature, which include:

- Solar operated cars – A solar car is driven by solar energy, obtained from solar panels placed on the surface of the car, or integrated solar cells into its body. The term solar cars mean that solar energy is used to power all or a part of a propulsion vehicle.
- Hybrid solar energy and electric operated cars – A hybrid car is a vehicle that uses two or more power sources to initiate the car. The term most commonly refers to HEVs, which combine solar energy and electric energy. Instead of using energy from solar panels, electric cars get their energy from batteries.
- Hybrid solar energy and internal combustion engine (ICE) operated car – Hybrid solar cars use a combination of the ICE and solar panels. The stored battery system powers the electric motor. A car is driven by a specified petrol engine and by solar energy obtained from solar panels [6].

In most of the solar cars, solar panels are located and fixed at almost a horizontal position. This solution, although it is the most practical, does not allow the maximization of net power from the sun. A moving panel would increase the solar contribution from about 46%, at low latitudes, up to 78%, at high latitudes. Also, to maximize the solar contribution, solar panels could be integrated into windows and to the lateral surface of a car [7]. Therefore, it seems that the installation of a movable solar roof and the use of solar panels on windows, side doors, and other accessible surfaces would allow a significant yield of solar energy. In the continued paper, they will be presented a various prototypes of solar cars and solar hybrids developed and made by well-known automobile companies, as well as prototypes of start-up companies whose primary goal is the mass production of solar cars.

1. DEVELOPMENT OF SOLAR VEHICLES

The development of solar cars in terms of the appearance of vehicles, weight, speed, and energy management in the last 20 years is astonishing. An Australian adventurer from Denmark Hans Tholstrup, in 1982, drove the world's first solar car. His passion for motorsport and the experience he gained during his travels inspired him to organize an event known as the World Solar Challenge or the Bridgestone World Solar Challenge (BWSC) from 2013. For more than 30 years, the world's largest solar event has been urging the

greatest minds from around the world to come to Australia to push the boundaries of technological innovation and test their solar-powered vehicle to travel 3,000 km from Darwin to Adelaide. In 2017, this event celebrated its 30th anniversary. The teams consist of high school and university students from over 30 countries. At the first event in 1987, 23 teams from seven countries were attending, and the winner was General Motors 'solar car, Figure 1 [7]. In 2019, 44 teams from 21 countries took part in the race, and the winner was the Belgian team The Agoria Solar Team with their solar vehicle BluePoint, Figure 2 [8, 9]. Over the last 20 years, the technological development of solar cars, which participated in BWSC, has shown that the aerodynamic shape of the vehicle and its weight are the two most important factors that influence the speed. These two areas made enormous progress. From the first organized event until today, the materials used to build solar cars have changed dramatically and evolved. The usage of composite materials, found in the aerospace industry, is common because these materials are extremely strong, and at the same time very light. The shape and appearance of solar cars have changed quite completely as the aerodynamic factor becomes a very strong influencing factor.

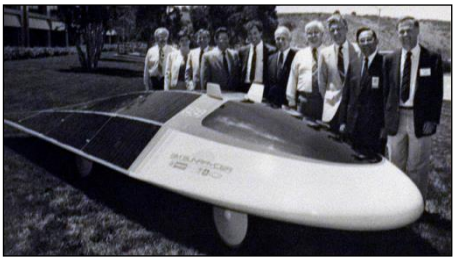

Figure 1 General Motors' team (1987) [7]

Figure 2 Agoria Solar Team (2019) [9]

To ensure that solar cars increase their practicality, event organizers are constantly introducing new regulations. So, present solar cars should have the appearance of "normal cars" with characteristics such as more upright seating, unobstructed entry and exit from the vehicle, lamps on the front and rear of the vehicle, etc. [10]. The organizers' idea is to build a solar car for everyday use.

2. CURRENT STATUS OF THE SOLAR TECHNOLOGY IN AUTOMOTIVE INDUSTRY

Automotive regulatory frameworks around the world were key for creating a sustainable environment in the automotive industry. In December 2018, the EU set new regulations for carbon dioxide emissions for new passenger cars and commercial vehicles. Regulation (EU) 2019/631 sets new EU fleet-wide CO_2 emission targets are set for the years 2025 and 2030, for newly registered passenger cars. These targets are defined as a percentage of car emission reduction starting from the 2021: 15% reduction until 2025 on and 37.5% reduction until 2030 [11]. Great expertise is needed in various fields, such as photovoltaics, electrical engineering and vehicle design, to install and to integrate solar photovoltaic panels and cells in a car. The Solar Vehicle Market is a comprehensive survey that provides information on the size, trends, growth, cost structure, capacity, revenue, and forecast of solar vehicles until 2026. The Global Solar Vehicle Market Report is available for international markets as well as development trends, competitive landscape analysis, and key development status of the region. It considers development policies and plans, as well as production processes and cost structures. The Global Solar Vehicle Market is segmented based on vehicle type, electric vehicle type, battery type, solar panel type, and geography,

Table 1 [12]. Main players in this field are Lightyear, Volkswagen, Toyota, Nissan, Ford, General Motors, Mahindra and Mahindra, Sono Motors, Hyndai, etc. Also, the report, "Solar Cars, Buses, Trucks, Trains 2020-2030" shows why a rapidly increasing number of car companies are incorporating solar bodywork that significantly increases range or reduces battery size [13].

Table 1 *Scope of the Global Solar Powered Vehicles Market*

Vehicle Type	Passenger Cars; Commercial Vehicles
Electric Vehicle Type	Battery Electric Vehicle; Hybrid Electric Vehicle
Battery Type	Lithium Ion; Lean Acid; Others
Solar Panel Type	Mono-Crystalline; Poly-Crystalline
Geography	North America (US, Canada, Rest of North America); Europe (Germany, UK, France, Spain, Rest of Europe); Asia Pacific (China, Japan, India, Rest of Asia-Pacific); Rest of the World (Brazil, UAE..)

2.1 Stella

Solar Team Eindhoven, a group of students from the Technical University of Eindhoven in the Netherlands, designed, constructed and built Stella Era [14].
The Stella Era is an experimental, solar car capable of traveling a distance of 1 800 km through more efficient use of solar energy, Figure 3. Equipped with Ericsson's Solar Smart parking, Stella Era car drives autonomously to a parking spot with the most sunshine to recharge its batteries [15]. In this way, it is enabled the maximum use of the available solar energy. It is also possible to share the energy with other electric vehicles parked next to it. In the morning, a car can transmit energy to the house to satisfy the energy needs of the users. The car also monitors the daily routines to make sure that the user had enough energy. The advantage lies in the aerodynamics, electrical efficiency, and weight of the car. Electrical efficiency has been significantly improved by developing a complete powertrain.

Figure 3 Stella Era [15]

Figure 4 Stella Era – energy exchange [15]

The most important parts are the two independent motors which reaching an efficiency of 98.5%. Energy exchange is possible only when solar energy collection is maximized, Figure 4 [15].
The Stella Lux is an energy-positive family car. Throughout the year, it generates more energy than it consumes. Aerodynamic design plays an important role in this fact. Namely, it seems that the tunnel passes through the car center, Figure 5. Besides, Stella Lux has an extended roof on both sides of the car, Figure 6. This made it possible to install another

series of solar panels on the car, which increases the energy yield. Stella Lux is extremely light. To accomplish this characteristic it was used material such as carbon fibres and aluminium. Solar cells are the most important component in powering a vehicle. A total of 381 monocrystalline silicon cells were combined to form a highly efficient solar array (module) (1.5 kW) with a total area of 5.84 m^2.

Figure 5 Stella Lux [16]

Figure 6 Extended roof [15]

Even when it is cloudy, the capture of sunlight is maximized by using a non-reflective surface made up of tiny prisms. These prisms bend the diffracted light to ensure that it arrives perpendicular to the solar cells, increasing the solar yield under all conditions. The solar array has demonstrated a maximum efficiency of up to 23.9%, which is very high in comparison with standard solar panels [16]. The custom-designed battery pack contains 1224 Lithium-Ion 3450 mAh battery cells, giving a total storage capacity of 15.2 kWh. The battery pack uses intelligent load balancing technologies to ensure an extremely efficient conversion of the stored energy. The battery monitoring system continuously checks the state of charge. With the combination of direct solar energy and the battery pack, the maximum daily range of the car is up to 1000 km in summer but varies with the time of the year. Placing the motors directly in the wheels means that no transmission or gearbox is needed, resulting in an energy efficiency of 96%. The total powertrain – consisting of the battery and motor – has a measured efficiency of 92% [17]. Stella Lux is a fully functional prototype.

During 2017, the students involved in making these vehicles started their own start-up company to make a commercially viable version of the car, called the Lightyear One.

2.2 Lightyear One

The Lightyear one is a vehicle that the Times magazine announced as one of the top 100 inventions for 2019. The Dutch company for solar cars, Lightyear, has designed the body of its vehicle to be as aerodynamic as possible at the same time, as well as to increase the space for installing solar cells. The Lightyear One is a lightweight car that has all-wheel drive, four doors, and that offers an exceptional range of 725 km on a relatively small battery, Figure 7.

Figure 7 Lightyear One [19]

According to the co-founder of the start-up company Lex Hoefslot, this car should be able to stay completely on solar energy for two months in the summer. The car has a unique design. There are about 1000 individual photovoltaic cells placed on the body of the car. Together, the roof and cover offer a stunning 5 m^2 of integrated solar cells in safety glass so strong that a fully grown adult can walk on them without causing dents. Lightyear One charges itself whenever the roof absorbs daylight. No matter whether you're driving or parked, the solar cells add up to 12 km of range per hour. If this car stays in the sun, it can reach an average of about 32 km of additional electric range per day. Conservative driving style, which includes slower acceleration, proper regenerative braking, and limited top speed, allows the car to have an even longer range. Due to the improved energy efficiency of the powertrain, it is required less energy for the same range. This improves the charging time by almost a factor of three. With power outlets available worldwide, the Lightyear One can be charged 440 km overnight (12 hours), anywhere [18]. The company predicted that there would be situations where the solar roof would be in the shade, so they included a 30% shadow factor to compensate for these losses. The Lightyear Platform uses a combination of aluminium and carbon fibre. One of the advantages of our architecture is there is no engine at the front of the car. Lightyear One has four in-wheel motors, providing power when and where needed. Working independently, they improve traction control on various surfaces and maximize efficiency. They have been able to increase the efficiency of the whole powertrain, making the Lightyear One the most efficient production car. One of the biggest achievements of this car is the low value of the aerodynamic drag. Current simulations show that this car will become the most aerodynamic production car [19]. Recent tests showed that the value of the drug coefficient (Cw), a measure of air resistance, will be below 0.20. Good aerodynamic performance ensures the reduced energy consumption. This is particularly advantageous when used frequently on motorways, especially when driving long distances or high speeds. Due to the lower energy consumption, the car has a greater range [20]. One of the key contributions to this achievement is the removal of physical side mirrors, which have been replaced by cameras.

At Lightyear one, the focus is on clear design, futuristic technology, and intuitive interaction. The first handmade production model will cost 149990 €. The start of production is in 2021 [21].

2.3 SionSono

Sono Motors is a new innovative car manufacturer founded in 2016, and has a vision of sustainable mobility that is not dependent on fossil fuels. Sono Motors is developing an advanced self-charging electric car with integrated solar cells, Figure 8 [22]. The CO_2 emission that cannot be avoided or reduced during the production and construction of the vehicle will be fully compensated. This company developed Sion 2017 prototypes. Solar cells are integrated on car entire surface, which completely redefines its appearance. The roof, side roof cover, fenders, and rear of the vehicle contain integrated solar cells, Figure 9.

Figure 8 Sion [23]

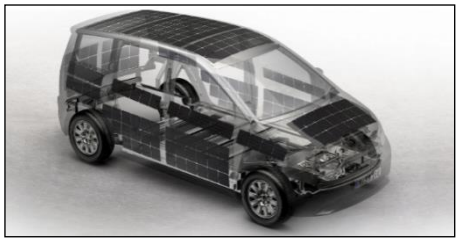

Figure 9 Integrated cells [24]

Sion thus becomes a solar electric vehicle (SEV), whose battery can be additionally charged by the power of the Sun. The cells are made of monocrystalline silicon and can produce energy even under clear skies or in the shade. In terms of top performance, integrated cells can generate up to 1.2 kW. The system is protected by a robust scratch-resistant polymer [23]. With solar cells integrated into the entire body of the car, Sion can easily charge the battery with the help of the Sun. So, in ideal conditions, up to 34 km of additional range per day can be achieved with pure solar energy, Figure 10.

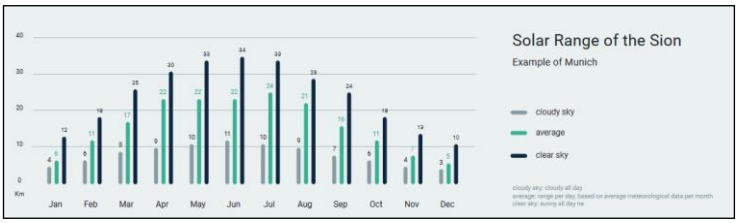

Figure 10 Solar range [24]

Sion solar panels are not unique just because of their lightweight. Innovative solar cell technology provides maximum efficiency and higher energy yield in small areas. The car has a lithium-ion battery, with a capacity of 35 kWh, which has water cooling. The battery capacity is sufficient for a range of 255 km. This car has a single-speed gearbox with a three-phase 120 kW synchronous motor. The speed of this car can easily reach 140 km/h. Sion can be charged at almost any charging station in Europe using any of three different charging modes: SchuKo (13 h), Type 2 (3.2 h), and CCS (fast-charging station 40 min).
Thanks to two-way charging technology, Sion can draw and store energy, and share it as well. Together with its partners, this company has developed a not only completely new technology for cell integration but also a device that enables the use of solar energy. The company calls this device "MPPT Central Unit". MPPT is a term for tracking maximum power commonly used in photovoltaic conditions. It is a process that adjusts the electrical load of the solar module so that the cells can give optimal performance. The prototype device developed by Sono Motors was tested earlier this year. Production will begin in the second half of 2021 and Zion will be produced in the former cult plant of the SAAB brand in Sweden. Sono Motors plans to produce 260,000 Sion over eight years [24].

2.4 Hyundai

Korean carmaker Hyundai has also applied solar energy to its cars. July 22, 2019 - Hyundai launches the Sonata Hybrid equipped with the world's first Active Shift Control (ASC) technology and solar roof system [25], Figure 11. This generation of models has a classic Sonata exterior design, but additionally includes an updated grille, a more precisely defined spoiler and, in particular, a solar roof.

Figure 11 Hyundai Sonata Hybrid [25]

The new 2020 Hyundai Sonata Hybrid has an eco-friendly solar roof system which charges car's battery using solar panels even while driving. The solar roof system improves fuel efficiency while preventing battery discharge and reducing CO_2 emissions. With this technology, 30 to 60 % of a car's battery can be charged via solar energy [26]. The solar roof system consists of the structure of silicon solar cells. The annual range can be increased up to 1300 km if the car is charged 6 hours per day [27]. The system consists of a solar panel and a regulator. After processing through various control mechanisms to increase efficiency, electricity is stored in both the starter battery and the drive battery, Figure 12. This electricity in the drive battery works to extend the driving distance, while that in the starting battery reduces the time required for the alternator to charge the starter, thus reducing the engine load and improving fuel efficiency [28].

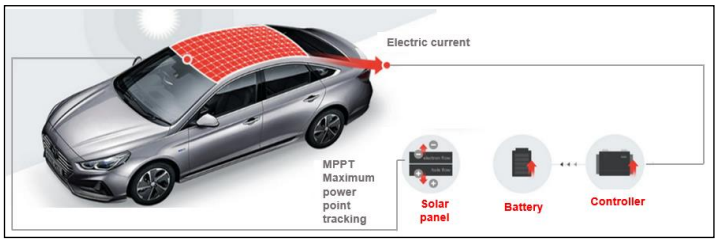

Figure 12 Hyundai Sonata Hybrid [25]

So far, Hyundai has only revealed the powertrain specifications of a model designed for the Korean market that consists of a 4-cylinder 2.0-liter internal combustion engine that produces 110 kW paired with an electric motor that produces 37 kW power. When working together, the total power of 145 kW is sent to all four wheels via a six-speed hybrid automatic transmission. ASC applies new control logic software to the hybrid control unit, which then controls the electric motor to match engine rotation and transmission speeds, ultimately reducing gear transmission time by 30%.

2.5 Toyota

Toyota does not currently produce purely electric vehicles (except Mirai with hydrogen), so these solar roofs are currently intended for plug-in hybrids. Toyota has positioned plug-in hybrid cars (PHVs) as the "pillars of next-generation of eco-friendly vehicles" alongside hybrid vehicles and has made significant efforts to strengthen its products [29]. Toyota, along with NEDO and Sharp, is leading an interesting research project on an electric car that uses a plug-in, equipped with a solar charging system, Figure 13. The idea is to assess how much energy can be provided by using highly efficient photovoltaic cells and how this corresponds to economic viability. The Japanese manufacturer decided to use Sharp's triple couplings solar cells in the form of a thin film (about 0.03 mm thick) with a conversion efficiency of up to 34%. A new Prius PHV model was used for this research, which has greatly developed environmental performance. Namely, this model has enough flexibility, not only on the roof of the car but also on the hood and its rear part, Figure 14. Toyota said that these panels have achieved conversion efficiencies of 34% or more and they are capable of delivering 860 W of power, which is roughly 4.8 times more than the commercially available Prius [30].

Figure 13 Toyota Prius [31]

Toyota will test the vehicle in different driving conditions to verify data such as the amount of solar panel electricity and the amount of charge of the drive battery, and the future charging of the solar devices in the vehicle.

Figure 14 Solar cells [31]

The demonstration vehicle was shown at the NEDO stand on "14. World Renewable Energy Exhibition" held in Pacific Yokohama in 2019. Prius PHV has solar battery cell conversion efficiency about 22.5% while demonstration vehicle has cell conversion efficiency about 34% [32].

2.6 Ford

It's been more than six years since Ford introduced its C-Max Solar Energy concept, Figure 15. The C-Max Solar Energy concept uses solar energy to directly charge the hybrid battery. In 2014, Ford introduced a rooftop solar system that tracks the movement of the sun and uses a Fresnel lens [33].

Figure 15 C-Max Solar Energy concept [35]

The car has a special concentrator that acts like a magnifying glass (Fresnel lens), which intensively directs the rays to the solar panels on the roof of the car [34]. This design helps increase the efficiency of the solar cells on the roof, which can also move to follow the sun as it moves across the sky. The Figure 16 represents how Ford's Solar Energy system works.

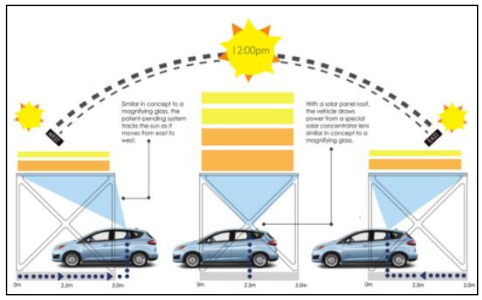

Figure 16 Ford's Solar Energy system [35]

Ford filed the patent application on November 8, 2019, and it was published on May 14, 2020. In this patent application, the roof-mounted shape of the switch stands out: a fabric with automatic covering with flexible solar cells with a thin layer that is controlled by a central shaft mounted on the rear bumper or in the trunk. The patent describes the concept as a flexible shield that unfolds using an inflatable pump and is powered by stored solar energy. The cover consists of flexible, thin-film solar cells that, once deployed, maintain shape using a memory polymer [36].

2.7 Tesla

So far, there has been no application of solar technology on Tesla cars. Elon Musk initially rejected the application of solar panels directly on cars. However, in November 2019, Musk announced that the new Tesla Cybertruck would be the company's first car which offers solar panels as an option to expand the range, Figure 17. The Tesla Cybertruck is an upcoming all-electric light commercial vehicle. There will be 3 models available with a range of 400 to 800 km and with the acceleration from 0-60 mph (0-97 km/h) of 6.5 to 2.9 seconds, depending on the model [37].

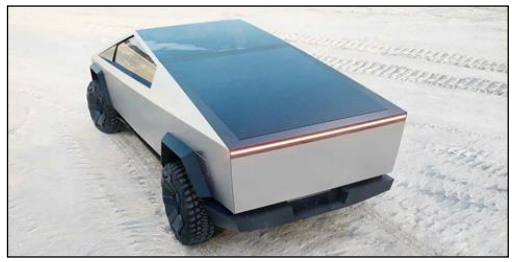

Figure 17 Tesla Cybertruck [38]

So far, there is no other information, except that production should start at the end of 2021.

3. COMPARATIVE ANALYSIS OF SOLAR VEHICLES

Fig. 18 shows driving ranges of solar vehicles: Stella Era, Lightyear One, and Sion.

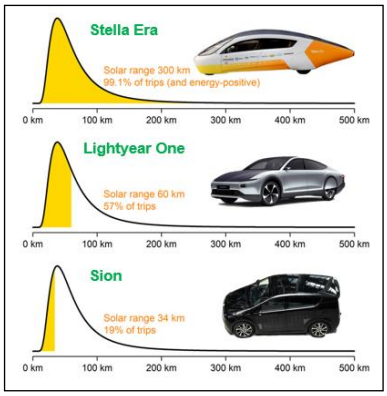

Figure 18 Solar range [39]

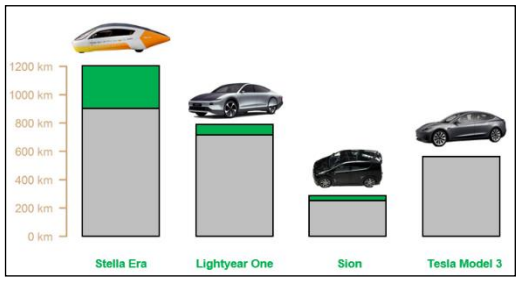

Figure 19 Driving ranges [39]

The Stella Era has a solar-only range for about 300 km (more than 4 times the mean 70 km driven). On more than 99% of trips, Stella Era can operate solar-only, and, on average, its solar panel produces substantial excess electricity which can be donated to other vehicles. Lightyear One has a solar-only range for about 60 km (less than the mean 70 km) but is still able to operate solar-only on 57% of trips. And Sion as a solar-only range for about 34 km, but Sion is able to operate solar-only on 19% of trips, and has a useful solar boost to its battery the rest of the time.

Figure 19 represents the driving ranges for four electric vehicles (grey for battery range, green for amplification due to the existence of solar panels). The four cars are Stella Era, Lightyear one, Zion, and non-solar model Tesla Model S. The Stella Era, in spite of having a much smaller battery pack, has almost double the range of the Tesla. This is due to the Dutch racing car's extremely aerodynamic shape and light carbon-fiber construction. Lightyear One comes about as close to the performance of Stella Era.

Fig. 20 and 21 represents a diagram which compares parameters and price of cars.

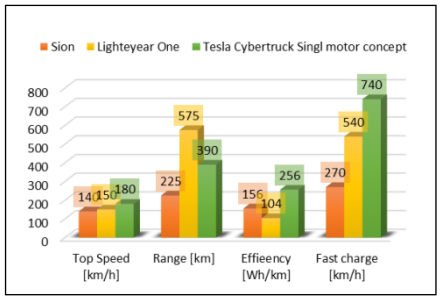

Figure 20 Parameters comparsion

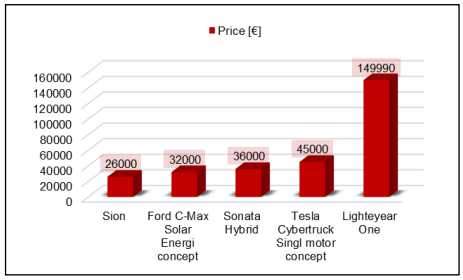

Figure 21 Price of cars

Figure 21 shows that the characteristics of the car differ significantly. For example, Lightyear One has a long-range, but also has a lower top speed, compared with other cars and alike. Also, figure 21 gives a comparison between cars for its price. Sion is the most affordable car, and Lightyear One is the most expensive car [39]. In the end, it is the buyer who determines which car to choose. The Sonata Hybrid solar roof has improved panel output and made the regulator more efficient, increasing the daily distance by 20% compared to the Toyota Prius. The one-day sonata ride is 3.6 km, which is more than the distance of 2.9 km announced by Toyota. Besides, the cost of a solar roof for the Sonata Hybrid is about 970 €, while the Prius is approximately 2250 €. Sonata's system is, in other words, more powerful, but twice economical as Prius'.

4. CONCLUSIONS

Our future clearly depends on our ability to utilize solar and other renewable sources of energy. Solar energy is a major renewable energy source with the potential to meet many of the challenges facing the world. The automotive industry has seen increased application of solar power. Many automobile manufacturers have attempted to use photovoltaic panels as an energy source for its cars. The application of solar energy on vehicles is becoming more feasible, that is why solar vehicles and hybrid solar vehicles may, therefore, represent a valuable solution to face both energy-saving and environmental issues. Although the development of these cars is based on well-known technologies, it is necessary to redesign and optimize the entire drive system to maximize its benefits. Also, it is necessary to pay special attention to maximizing the net power of solar panels and managing the obtained energy. In addition to the fact that the potential benefits of solar energy are clear, its limitations are also clear, which are occasional and which arise due to the influence of the relative movement between the Earth and the Sun and due to changes in weather conditions.

ACKNOWLEDGMENTS

This investigation is a part of the projects TR 33015 and III 42013. The authors would like to thank to the Ministry of Education and Science of Republic of Serbia for the financial support during this investigation.

REFERENCES

[1] Cairns, E.: "A new mandate for energy conversion: zero emission (electric) vehicles", International Power Sources Symposium, New Jersey, 1992, pp. 310-313.

[2] Maggeto, G., Van Mierlo, J.: "Electric and electric hybrid vehicle technology: a survey", IEE 35th Seminar on Electric, Hybrid and Fuel Cell Vehicles, 2000, pp. 1/1-11.

[3] Matsumoto, S.: "Advancement of hybrid vehicle technology", European Conference on Power Electronics and Applications, Germany, 2005, -7.

[4] Rizzo, G., Arsie, I., Sorrentino, M.: "Solar energy for cars: perspectives, opportunities and problems", GTAA Meeting, Mulhouse, 2010, Vol. 43, No. 7, pp. 174-185.

[5] Spina, M., de la Vega, R., Rossi, S., Santillán, G., Leegstra, R., Verucchi, C., Gachen, F., Romero, R., Acosta, G.: „Some Issues on the Design of a Solar Vehicle Based on Hybrid Energy System", International Journal of Energy Engineering, United States, 2012, Vol. 2, No. 1, pp. 15-21.

[6] Singh, R., Gaur, M., Malvi, C.: "Study of Solar Energy Operated Hybrid Mild Cars: A Review", International Journal of Scientific Engineering and Technology, India, 2012, Vol.1, No. 4, pp. 139-148.

[7] Chips Etc, GM "Sunraycer" Solar Powered Race Car Paperweight (1987), https://www.chipsetc.com/gm---general-motors.html, accessed: 29.05.2022.

[8] Bridgestone World Solar Challenge, https://www.worldsolarchallenge.org/, accessed: 01.06.2020.

[9] Agoria Solar Team, https://www.solarteam.be/, accessed: 01.06.2022.

[10] World Solar Challenge: "2019 Regulations", 2018, https://www.worldsolarchallenge.org/files/2272_2019_bwsc_regulations_release_version_3.pdf, accessed: 01.06.2022.

[11] European Commission, Regulation (EU) 2019/631 of the European Parliament and of the Council of 17 April 2019 setting CO_2 emission performance standards for new passenger cars and for new light commercial vehicles, and repealing Regulations (EC) No 443/2009 and (EU) No 510/2011).

[12] Imarc Group: "Global Industry Trends, Share, Size, Growth, Opportunity and Forecast 2020-2025", 2020.

[13] Harrop, P.: "Solar Cars, Buses, Trucks, Trains 2020-2030", IDTechEx Research.

[14] Papaliouras, I.: "Design and implementation of adaptive cruise control system for the TU/e solar powered electric car", TechnischeUniversiteit Eindhoven, 2016, p.100 .

[15] Solar TeamEindhove, https://solarteameindhoven.nl/, accessed: 02.06.2022.

[16] Selten, T.: "Stella Lux: the energy-positive family car", Europhysics News, 2017, Vol. 48, No. 3, pp. 13-16.

[17] Rutten, B., Cobbenhagen, R.: "Future Trends in Electric Vehicles Enabled by Internet Connectivity, Solar, and Battery Technology", Automotive Systems and SoftwareEngineering,Springer, Cham, 2019, pp. 323-346.

[18] Mini Brochure, Lightyear One, https://www.gcnl.nl/resources/uploads/2019/10/Mini-Brochure-Lightyear-One_082019_smaller4992.pdf, 04.06.2022.

[19] Lightyear, Lightyear, https://www.qualenergia.it/wp-content/uploads/2019/02/Lightyear-One-Car-Brochure-Online-Version.pdf, accessed: 04.06.2022.

[20] Mester, G., Egyetem, Ó., Iskola, B.: "Mester Gyula Elektromos autok ujdonsagai 2019", Bánki Közlemények, 2019, Vol. 3, No. 1, pp. 37-41.

[21] Lightyear One, https://lightyear.one/, accessed: 04.06.2022.

[22] Bialic, E., Chappaz, C., Edme F.: "Intelligent Transportation Systems & Photovoltaic LiFi Communication Solution", Advanced R&D division, Sunpartner Technologies, Franc, 2018, pp. 1-6.

[23] Sono Motors, Information Sheet Sono Motors, 2019, https://sonomotors.com/site/assets/files/1621/information_sheet_sion_en.pdf, accessed: 06.06.2020.

[24] Sono Motors, https://sonomotors.com/, accessed: 06.06.2022.

[25] Hyundai, https://www.hyundai.com, accessed: 06.06.2022.

[26] Oosthuizen, C., Van Wyk, B., Hamam, Y., Desai, D., Alayli, Y., Lot, R.: "Solar Electric Vehicle Energy Optimization for the Sasol Solar Challenge 2018", EEE Access, Australia, 2019, Vol. 7, No. 1, pp. 175143-175158.

[27] Hyundai, 2020 Sonata Hybrid, https://www.hyundaiusa.com/us/en/vehicles/2020-sonata-hybrid, accessed: 07.06.2022.

[28] Hyundai motor group, Solar Roof: Car Roofs that Generate Energy https://news.hyundaimotorgroup.com/Article/What-does-a-solar-roof-do-A-car-roof-that-generates-energy, accessed: 09.06.2022.

[29] Toyota, https://global.toyota/, accessed: 09.06.2022.

[30] Giovanni, D., Sutantra, I.: "Mapping of operating modes, power flows and analysis of tractive force characteristics of series – Parallel plug-in hybrid vehicle in certain driving cycle (Case study: Toyota Prius Plug-in Hybrid)", AIP Conference Proceedings, United States, 2019, Vol. 2187, No. 1, pp. 050009.

[31] Green car reports, Toyota covers Prius Prime with solar panels to test mileage, https://www.greencarreports.com/news/1123920_toyota-covers-prius-prime-with-solar-panels-to-test-mileage, accessed: 10.06.2022.

[32] Arias, J.: "Solar Energy, Energy Storageand Virtual Power Plantsin Japan - Potential Opportunities of Collaboration between Japanese and European Firms", 2018, Toykio, https://www.eujapan.eu/sites/default/files/publications/docs/min18_1_arias_solarenergy-energystorageandvirtualpowerplantsinjapan.pdf, accessed: 11.06.2020.

[33] Ford Motor Company, https://media.ford.com/, accessed: 11.06.2022.

[34] Vu, N., Pham, T., Shin, S.: "Flat concentrator photovoltaic system for automotive applications", Solar Energy, Elsevier, 2019, Vol. 190, pp. 246-254.

[35] Clean Technica, Ford C-Max Solar Energi Concept Car Coming To CES 2014, https://cleantechnica.com/2014/01/02/ford-c-max-solar-energi-concept-car-coming-ces-2014/, accessed: 13.06.2022.

[36] Fordauthority, New Ford Patent Depicts A Wild, Inflatable, Solar-Powered EV Charging Bubble, https://fordauthority.com/2020/05/new-ford-patent-depicts-a-wild-inflatable-solar-powered-ev-charging-bubble/, accessed: 14.06.2026.

[37] Tesla, source: https://www.tesla.com/, accessed: 14.06.2022.

[38] Electrek, Tesla Cybertruck will have solar roof option to add 15 miles of range per day, https://electrek.co/2019/11/22/tesla-cybertruck-solar-roof-option-add-range/, accessed: 14.06.2022.

[39] WordPress, Solar-racing, https://scientificgems.wordpress.com/category/solar-racing/page/2/, accessed: 14.06.2022.

MOBILITY & VEHICLE MECHANICS

https://doi.org/10.24874/mvm.2022.48.03.04
UDC:629.3.018

EVALUATION OF THE ROLLOVER THRESHOLD OF TANK VEHICLES

Clio Vossou [1], Ioannis Katsas [2], Dimitrios Koulocheris [3]*

Received in August 2022 *Revised in September 2022* *Accepted in September 2022*
RESEARCH ARTICLE

ABSTRACT: The improvement of the driving safety and the eradication of accidents is a matter of high priority in research in the area of automotive engineering. Especially in heavy vehicles transporting dangerous goods, every accident means high cost due to probable loss of life, environmental pollution and infrastructure damage. The present paper focuses on the analysis of the dynamic behavior of tank vehicles used to transport flammable liquids. Its main purpose is to correlate the rollover threshold of tank vehicles to the geometry of the cross section of the tank taking into consideration the maximum allowed dimensions and gross weight. Firstly, a 4-axle truck is simulated using the multi-body software TruckSim® in order to monitor its dynamic behavior. Several simulation tests consisting of typical maneuvers were carried out considering different shapes of the cross section of the tank, considering equal volume of transported flammable liquid. For each simulation test several dynamic quantities have been monitored in order to estimate the safety against tank vehicle rollover. The results, among others, showed that the cross section providing the highest rollover threshold was an elliptical which looks like the box shaped. Furthermore, an important outcome of this paper is the determination of the maximum speed for each simulated maneuver and shape of cross section.

KEY WORDS: *tank vehicle, rollover, dynamic stability, tank cross section*

[1]*Clio Vossou, Researcher, National Technical University of Athens, School of Mechanical Engineering, Vehicles Laboratory, Greece, Zografou Campus, Iroon Polytexneiou 9, 157 80, klvossou@mail.ntua.gr*, ORCID ID: - 0000-0002-4665-7759 *(*Corresponding author)*
[2]*Ioannis Katsas, Student, National Technical University of Athens, School of Mechanical Engineering, Vehicles Laboratory, Greece, Zografou Campus, Iroon Polytexneiou 9, 157 80*, ORCID ID: -
[3]*Dimitrios Koulocheris, Assoc. prof., National Technical University of Athens, School of Mechanical Engineering, Vehicles Laboratory, Greece, Zografou Campus, Iroon Polytexneiou 9, 157 80, dbkoulva@mail.ntua.gr*, ORCID ID: 0000-0002-1379-5805

OCENA PRAGA PREVRATANJA VOZILA CISTERNE

REZIME: Poboljšanje bezbednosti u vožnji i iskorenjivanje nezgoda je pitanje visokog prioriteta u istraživanju u oblasti vozila. Naročito kod teških vozila koja prevoze opasne materije, svaka nezgoda znači visoku cenu zbog verovatnog gubitka života, zagađenja životne sredine i oštećenja infrastrukture. Ovaj rad se fokusira na analizu dinamičkog ponašanja cisterni koja se koriste za transport zapaljivih tečnosti. Njegova osnovna namena je da poveže prag prevrtanja vozila cisterne sa geometrijom poprečnog preseka rezervoara uzimajući u obzir maksimalno dozvoljene dimenzije i bruto težinu. Prvo, 4-osovinski kamion se simulira pomoću softvera za više karoserija TruckSim® kako bi se pratilo njegovo dinamičko ponašanje. Urađeno je nekoliko simulacionih testova koji se sastoje od tipičnih manevara s obzirom na različite oblike poprečnog preseka rezervoara, s obzirom na jednaku zapreminu transportovane zapaljive tečnosti. Za svaki simulacioni test je praćeno nekoliko dinamičkih veličina kako bi se procenila bezbednost od prevrtanja vozila cisterne. Rezultati su, između ostalog, pokazali da je poprečni presek koji obezbeđuje najviši prag prevrtanja eliptičan koji izgleda kao kutija. Nadalje, važan ishod ovog rada je određivanje maksimalne brzine za svaki simulirani manevar i oblik poprečnog preseka.

KLJUČNE REČI: *vozilo cisterna, prevrtanje, dinamička stabilnost, presek rezervoara*

EVALUATION OF THE ROLLOVER THRESHOLD OF TANK VEHICLES

Clio Vossou, Ioannis Katsas, Dimitrios Koulocheris

INTRODUCTION

According to Eurostat [1], the share of dangerous goods road transport (in tkm) for 2019 and 2020 was around 4% in both years compared to the total transport. Since 2015 the transport of dangerous goods in EU fluctuated. More specifically, between 2015 and 2019, 11 member states registered an increase in the transport of dangerous goods. The highest increases were recorded for Slovenia (74.8%), Croatia (+55.4%) and Italy (+32.7%). Flammable liquids accounted for more than half of the transport of dangerous goods in the years of 2019 and 2020 [1]. Flammable liquids are usually transported with the use of tank vehicles. Tank vehicles that carry flammable liquids can be either articulated vehicles such as tractor-semitrailer or just tank trucks. If such a vehicle is involved in an accident the consequences are going to be important for the driver and the environment [2] due to both its high weight and the inherent danger of the transported material.

The most usual cause of a heavy vehicle accident is rollover; hence a lot of research has been done in order to improve the lateral stability of heavy vehicle and avoid a rollover accident. Bai Zhenyuan et. al [3] proposed a method of improving the lateral stability of a semi-trailer by using additional yaw moment of it. Dhruv Oberoi [4] developed an anti-roll control and optimized it in order to obtain better roll stability and directional performance of an articulated vehicle. However, it is very common especially, in small or developing countries, to transport flammable liquids like petrol (UN1202) and gasoline (UN1203) with tank trucks. Tian Xin et. al [5] has presented a research on the speed thresholds of trucks in a sharp turn based on dynamic rollover risk levels. Furthermore, Shimanovsky et. al [6] explained how baffles affect the dynamics of tank trucks which carry viscous liquids.

In this paper, the dynamic behaviour of a 4-axle tank truck with four tanks with geometrically different cross-sections is evaluated in TruckSim ® software. The dynamic behaviour of the tank truck is investigated in two different scenarios, tilt table and double lane change. Moreover, the dynamic response of the tank truck with each cross section in double lane change has been investigated with three different initial velocities and four different filling ratios.

1. MATERIALS & METHODS

For the analysis of the dynamic behaviour of heavy vehicles through numerical simulations TruckSim ® software is used. This software consists of three parts, the VS (VehicleSim) Browser (GUI), the VS Solver and the VS Visualizer and it utilizes ordinary differential equations (ODE) [8]. The equations simulate the choices made at the user interface (VS Browser) while the solution is coming from the VS Solver. Through VS Visualizer the results are presented in video and plot format. Using TruckSim, the user can select the technical characteristics of the heavy vehicle, the scenario and the driving conditions, for example the wind velocity.

1.1 Heavy vehicle model

In this paper, a 4-axle tank truck is used for the simulation of two different scenarios. In Figure 1 the tank truck model is presented.

Figure 1 Vehicle model

The technical characteristics of the vehicle such as masses, types of suspensions and its mechanical properties and the tires are the ones that the software has as default. In Table 1, the values of the sprung and the unsprung mass of the heavy vehicle are presented.

Table 1 *Sprung and unsprung mass of the vehicle*

Sprung mass (kg)	4455
Center of unladen sprung mass	(X, Y, Z) = (1175, 0, 1115) from the origin of sprung mass
Unsprung mass (kg)	
Steering axle	174
Driving axle	603
Tyre (Steering)	91
Tyre (Driving)	91
Total unsprung mass	2646

In Table 2 the mechanical properties of the suspension on each axle are presented

Table 2 *Mechanical properties of the suspensions*

	Spring rate [N/mm]	Damper rate [kN/(m/s)]	Technical capacity [tonnes]
Axle 1 (Solid)	200	10	4
Axle 2 (Solid)	200	10	4
Axle 3 (Dual tires - Drive)	700	30	15.5
Axle 4 (Dual tires - Drive)	700	30	15.5

The engine of the vehicle is an internal combustion Diesel engine with 225 kW power at 2100 rpm. The transmission is automatic with 5 speeds and the shifts are made at 2100 rpm. The duration of the shift is 0.25 s.

1.2 Metallic Tank

Instead of the rectangular container shown in Figure 1, the tank vehicle has a metallic tank in order to transport the flammable liquid. This tank, according to EN13094 [9], can have a circular, an elliptical or a box-shaped cross-section. The box-shaped cross section consists of three circles of different radius.

In order to study the effect of the geometry of the cross section of the tank to the stability of the heavy vehicle, four different cross sections have been constructed in Solidworks

3DCAD software (Figure 2). Starting from a box-shaped cross section, the total volume of the tank has been calculated (28187 lt) and one equivalent (of the same volume) circular and two elliptical ones have been designed.

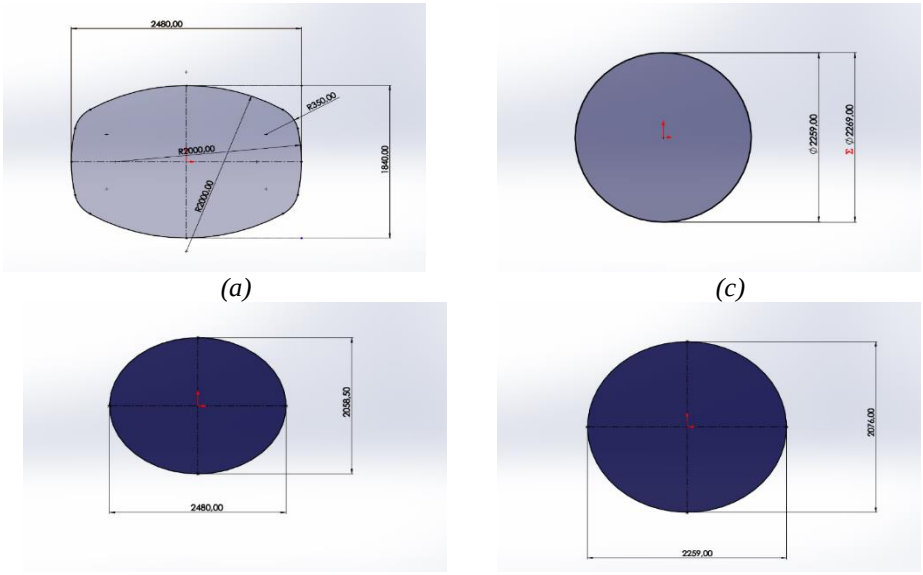

(a) *(c)*

(b) *(d)*

Figure 2 2D Sketch for the cross section (a) box shaped (M1) (b) circular (M2) (c) elliptical (M3)which looks like the circular (d) elliptical (M4) which looks like the box shaped

In Table 3 the main dimensions of each tank are presented.

Table 3 *Main dimensions of each tank*

Model	Cross-section	Width (mm)	Height (mm)	Length (mm)	Capacity (lt)
M1	Box-Shaped	480	840	595	28422
M2	Circular	259	259	070	28336
M3	Elliptical	259	076	636	28125
M4	Elliptical	480	058.5	070	28347

In Table 4 the net weight of each tank, constructed of sheets of aluminium alloy with thickness equal to 5 mm is presented. The density of the aluminium alloy is equal to 2700 kg/m3.

Table 4 *Net weight of each tank*

Model	Net Weight (kg)
1	792
2	788
3	704
4	683

In TruckSim ® the different tanks have been defined through the Payload definition screen presented in Figure 3. For each tank the position of its center of mass has to be defined along with the corresponding inertia of each cross- section.

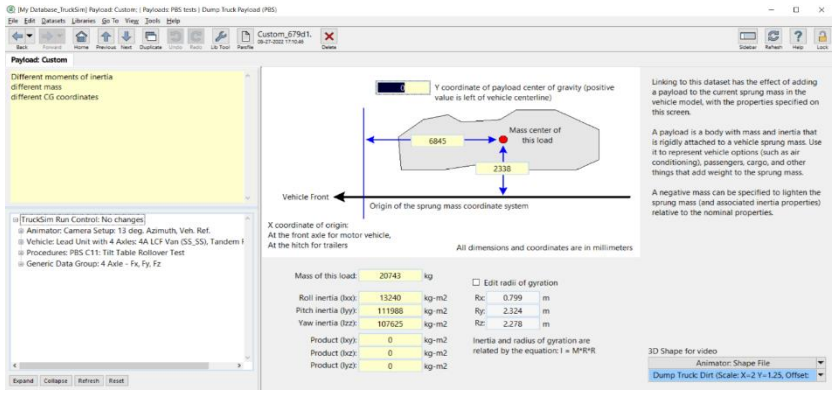

Figure 3 Payload definition in TruckSim

In Table 5 the position of the centre of mass for each tank on the x-z plane is presented. The origin for the measurements of these coordinates is the origin of the sprung mass.

Table 5 *Position of center of mass for each cross section*

Model	X-axis	Z-axis
1	6803 mm	2220 mm
2	6535 mm	2429,5 mm
3	6845 mm	2338 mm
4	6535 mm	2329 mm

Furthermore, in Table 6, the moments of inertia change according to the shape of the cross-section of the tank are presented.

Table 6 *Moments of inertia for each cross section*

Moment (kg·m^2)	M1	M2	M3	M4
Ixx (Roll)	14336	14497	13240	14687
Iyy (Pitch)	103829	99966	111988	97416
Izz (Yaw)	103123	95201	107625	95244

In order to calculate the mass of load, i.e. the mass of transported liquid, UN1203 has been considered, with density equal to 750 kg/m^3.

1.3 Driving scenarios

In order to evaluate the dynamic behaviour of the tank truck with the different tank cross-sections two different scenarios have been simulated. The first scenario is the quasi-static a tilt-table test [7]. During this test, the vehicle is fully loaded and mounted on a table with its longitudinal axis parallel to an axis that gradually tilts about the table. The simulation stops when the vehicle becomes unstable in roll.

Actually, every non-zero tilt angle simulates a non-vibratory steady state turn. The scope of this test is to define the steady-state rollover threshold of the vehicle, i.e., the maximum lateral acceleration the vehicle could deploy in steady state turn without rolling over [10]. The tilt rate is equal to 0.2^o/s. The variables of interest are the roll angle and the lateral acceleration. The second driving scenario is double lane change. During this scenario, the vehicle, having an initial velocity, changes lane twice in opposite directions and in short time. During this scenario, roll angle, lateral acceleration, yaw rate and vertical tire forces are monitored.

All the above-mentioned values as well as the scenarios are input in the software through the Run Control Interface that is presented in Figure 4.

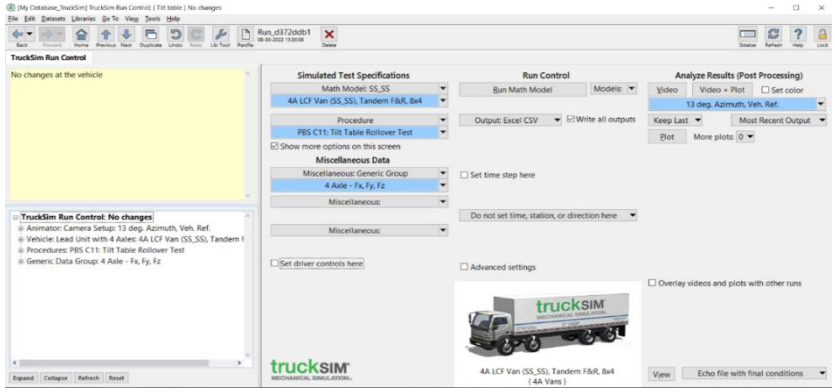

Figure 4 TruckSim Run Control interface

2. RESULTS

Firstly, the results for the scenario of tilt table test are presented for all the cross-section shapes. Then the double lane change scenario with constant velocity 30 km/h and 95% of the maximum payload for every tank cross section is presented.

2.1 Tilt-table test method

In the Figure 5 (a) the change in roll angle against time is presented for all cross-sections while in Figure 5 (b) the lateral acceleration versus time is presented.

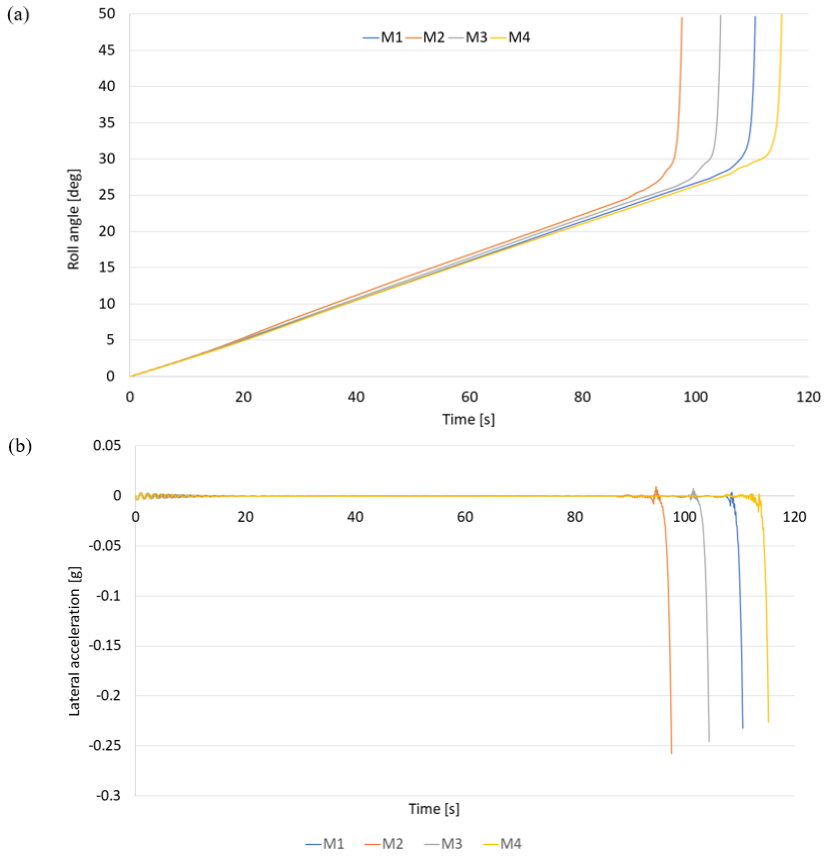

Figure 5 (a) Roll angle and (b) Lateral acceleration in tilt table test method

In Figure 5 (a) is obvious that the last cross-section to overturn is M4 followed by M1.

Rollover threshold is the maximum value of lateral acceleration a vehicle can sustain during steady-state cornering on a flat surface without rolling over [7]. The calculation for the rollover threshold is based on the equation:

$$Rollover\ threshold = \frac{mg \sin \varphi_C}{mg \cos \varphi_C} = \tan \varphi_C$$

where φ_C: tilt table angle the moment of critical wheel lift

Critical wheel lift is defined as the moment, in s, when the vehicle has a lateral acceleration equal to the rollover threshold [7], which is the moment of the first loss of contact of one axle to the tilt-table. Thus, the equilibrium at the roll plane cannot be established. Usually, the first axle which loses the contact with the table is one of the driving one. The rollover threshold of every cross section is presented in the Table 7.

Table 7 *Tilt table test results*

Model	Critical wheel lift [s]	First loss of contact	Time of Rollover [s]	**Rollover threshold [g]**
M1	102.0	Axle 3	108.5	0.37
M2	87.4	Axle 3	94.7	0.32
M3	96.1	Axle 3	101.5	0.35
M4	105.4	Axle 3	113.6	0.39

2.2 Double lane change

In the Figure 6, the most important dynamic quantities for the double lane change driving scenario are presented.

(a)

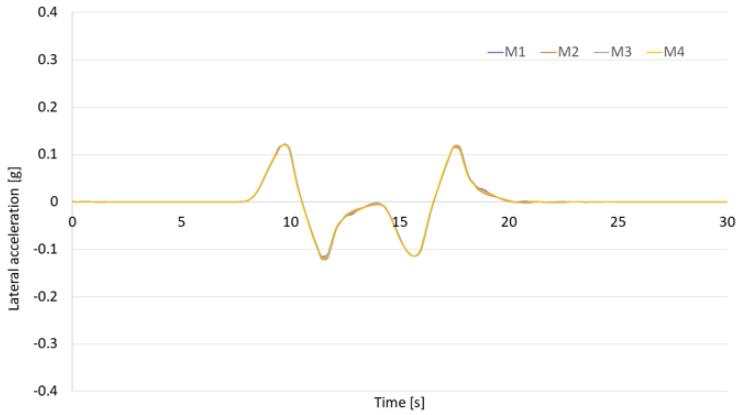

(b)

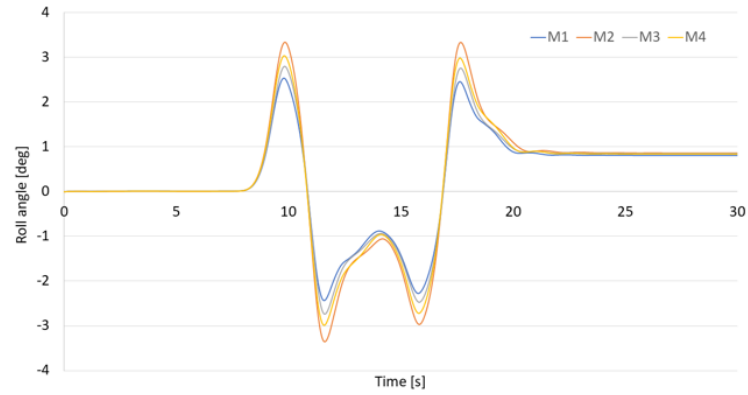

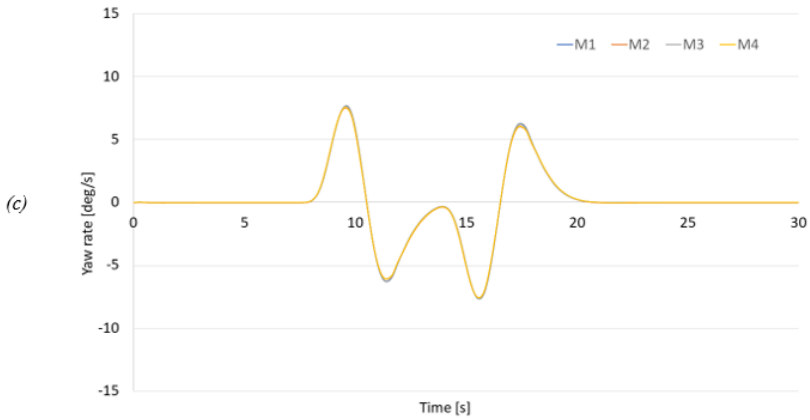

Figure 6 (a) Lateral acceleration, (b) roll angle and (c) yaw rate in double lane change with constant velocity 30 km/h

In Figure 6, is obvious that there is no effect of the cross-section geometry of the tank in the lateral acceleration and the yaw rate of the vehicle while there is a slight difference on the maximum and minimum values of the roll angle during each lane change.

Furthermore, the distribution of the weight of the tank truck in each axle has been investigated and presented in Table 8. The load was monitored in each axle through the vertical forces acting on the wheels during the phase of driving on a straight path i.e. after 22 s when the at steady state has been accomplished.

Table 8 *Axle load for each cross section*

Cross section	Forces per Axle (N)				Total load [kg]
	1	2	3	4	
M1	25952	26109	10966	11522	27987
M2	30570	30706	07262	07735	28065
M3	25172	25332	11448	12017	27928
M4	30577	30712	06781	07251	28162

For M1 and M3 cross sections, the front load axle (Axle 1) is lower compared to this of M2 and M4. On the other hand, the rear load axle (Axle 4) is larger. The last column in Table 8 is the total weight of the vehicle equipped with a tank of the corresponding cross section and 95% of the maximum capacity payload.

Total load = Sprung mass + Unsprung mass + Tank net weight + Transported Liquid weight.

3. DISCUSSION

The results of the first scenario showed that the rollover threshold resulting from tilt-table test is highly dependent on the geometry of the cross-cross section of the tank. On the other

hand, the results of the second scenario did not show such dependency. In order to further investigate the effect of the tank cross-section to the lateral stability of the tank truck during double lane change two more velocities have been simulated.

3.1 Parametric study of constant velocity

In both velocities (50 km/h and 70 km/h) the roll angle, the lateral acceleration and the yaw angle are presented for 50 km/h (Figure 7).

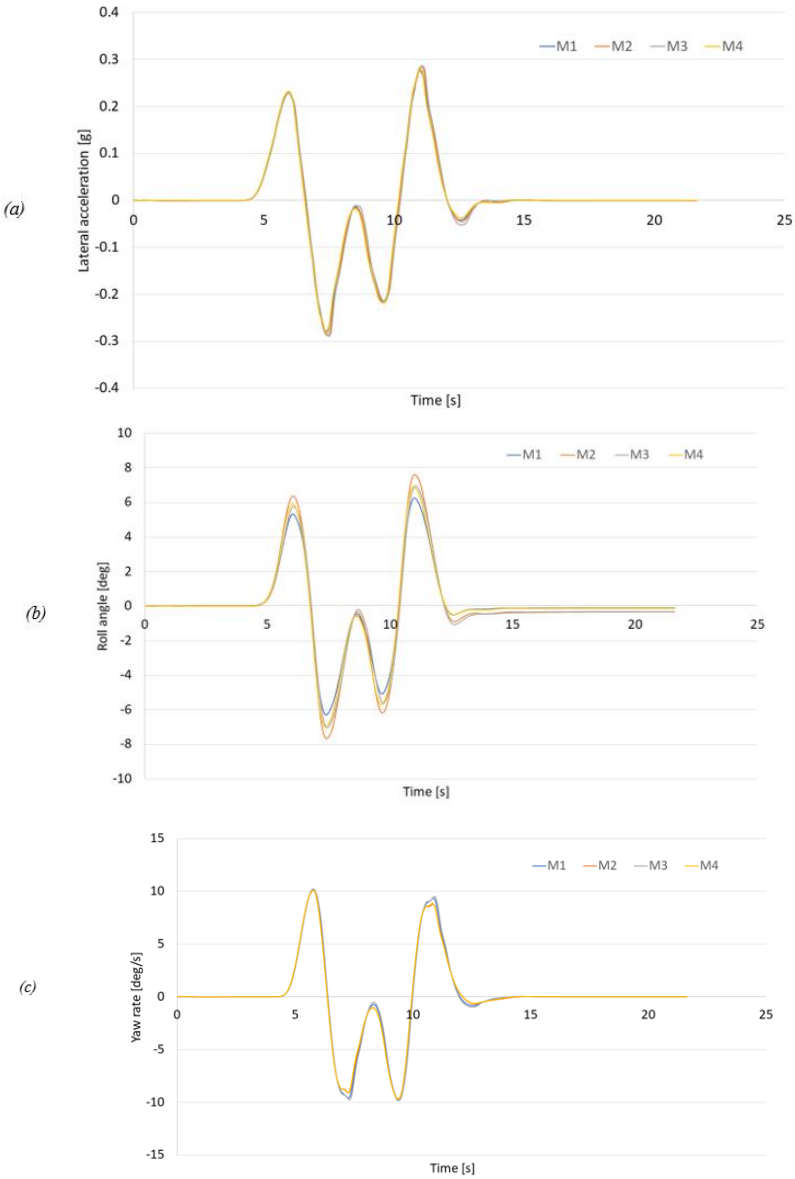

Figure 7 (a) Lateral acceleration (b) Roll angle (c) Yaw rate in double lane change with velocity 50 km/h

In Figure 8 the same dynamic quantities are presented for constant velocity of 70 km/h.

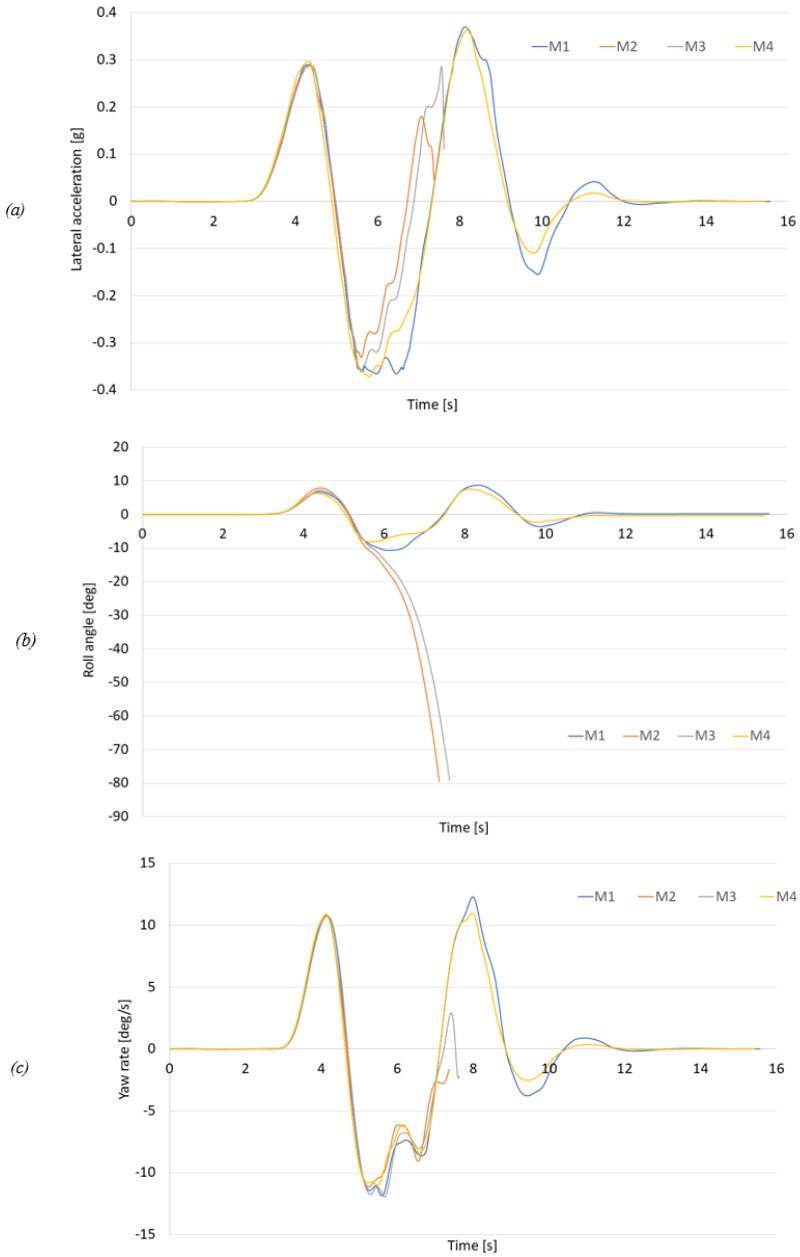

Figure 8 (a) Lateral acceleration (b) Roll angle (c) Yaw rate in double lane change with velocity 70 km/h

In Figure 8 (a) and (b), for constant velocity of 70 km/h, is obvious that the tank truck with tank cross-sections M2 & M3 rollover after almost 6 s and after the first lane change. In Figure 7 there is no overturn but the increase in velocity causes an increase of the minimum and maximum values. In Figures 9, 10 and 11 the maximum and minimum values of lateral acceleration, roll angle and yaw rate are presented for all constant velocities (30 km/h, 50 km/h and 70 km/h).

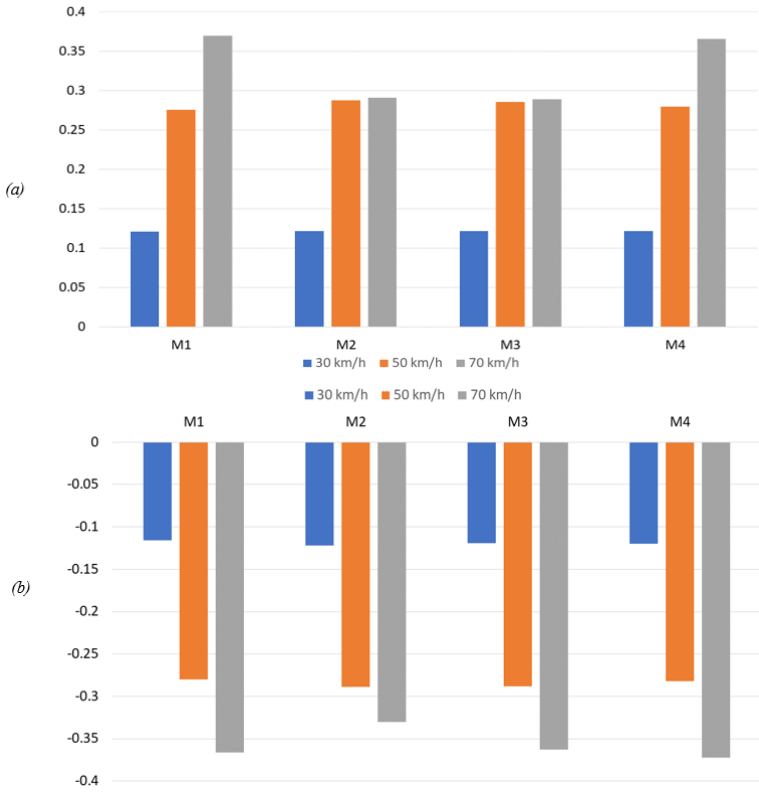

Figure 9 (a) Positive (b) Negative lateral acceleration in double lance change driving scenario for 30,50 and 70 km/h

For the cross sections M1 and M4, the absolute maximum values of the lateral acceleration increase as the velocity increases. Nevertheless, for the cross sections M2 and M3, the transition from 50 to 70 km/h does not affect the maximum and minimum values, only the dynamic behaviour, since rollover happens.

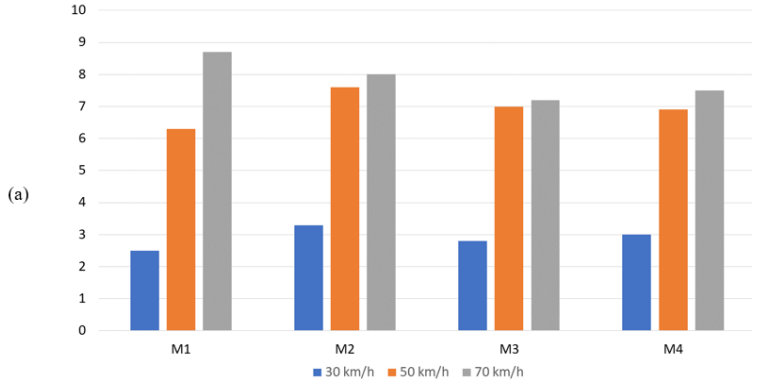

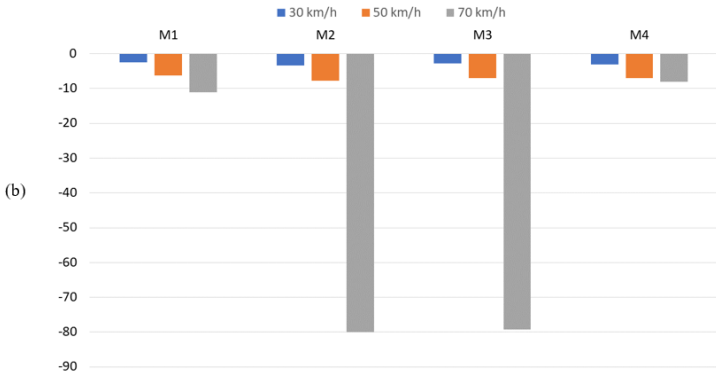

Figure 10 (a) Positive (b) Negative roll angle in double lance change driving scenario for 30,50 and 70 km/h

The results for the roll angle, in Figure 10, are similar to the ones for the lateral acceleration. Increasing velocity creates higher value of the roll angle. Again, is pointed out that the cross sections M1 and M4 carry out successfully the double lane change with every velocity. On the other hand, the cross sections M2 and M3 at velocity 70 km/h rollover.

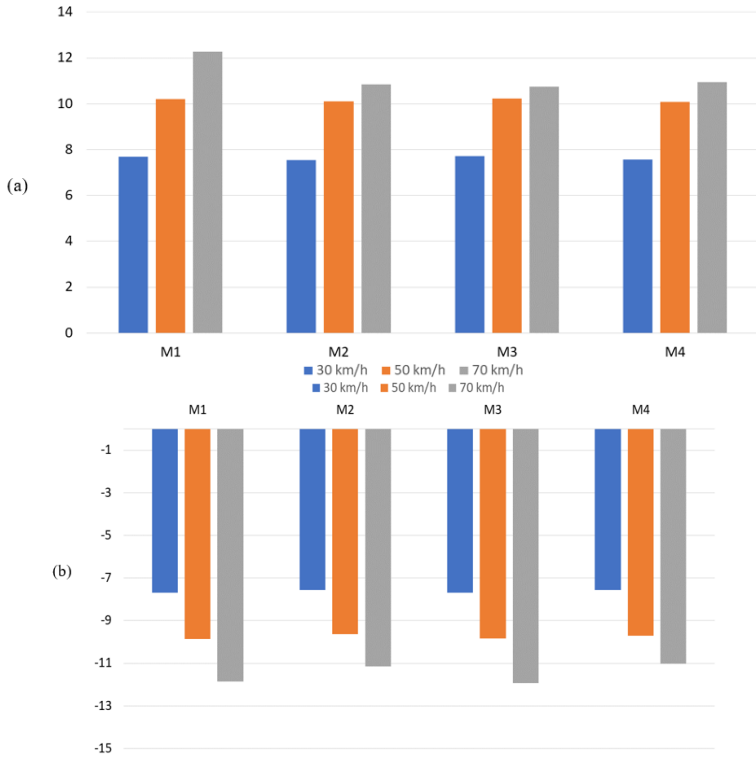

Figure 11 (a) Positive (b) Negative yaw rate in double lance change driving scenario for 30,50 and 70 km/h

The yaw rate, in Figure 11, does not change versus the velocity and does not seem to be affected by the geometry of the cross-section of the tank.

3.2 Parametric study of filling ratio

Since M2 and M3 rollover during double lane change with 70 km/h a parametric study of the degree of filling has been considered for M1 and four different degrees of filling, namely, 0% - 20% - 80%- 95%.

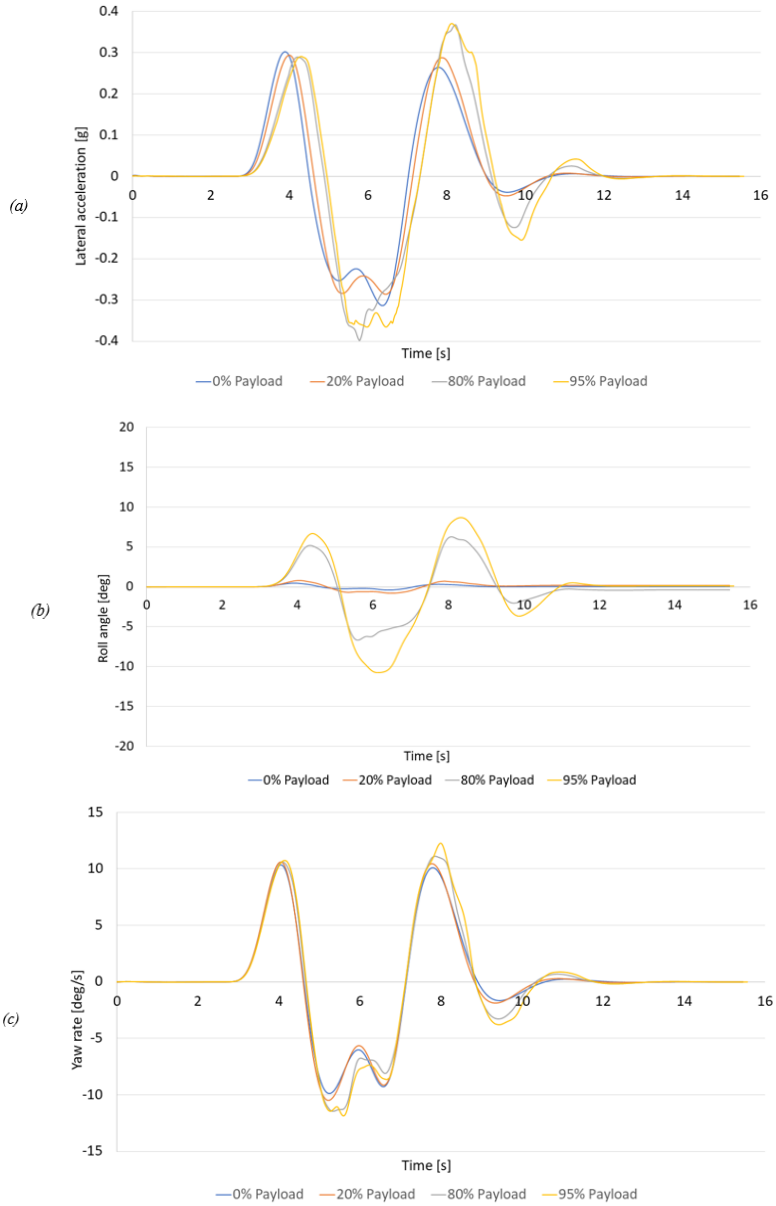

Figure 12 (a) Lateral acceleration (b) Roll angle (c) Yaw rate in double lane change with 4 different payload conditions, 0%-20%-80%-95%

In Figure 12 is shown that as the filling ratio increases the more difficult it is to avoid rollover. However, the M1 cross section is a safe option even if driving with 70 km/h and fully loaded truck. In the first lane change, the lateral acceleration and yaw rate are

approximately the same regardless the payload. Changing from 20% to 80% filling ratio makes the vehicle heavier and dynamically unstable. In other words, the vehicle starts oscillating after the first lane change with lateral acceleration close to 0.4g and roll angle close to 10 degrees but at the end, it returns to its safe steady-state.

4. CONCLUSIONS

In the present paper, the effect of the geometry of the cross section of a tank for the transport of flammable liquids in the rollover threshold of the heavy vehicle has been performed. The heavy vehicle has been a 4-axle tank truck and it has been tested in two scenarios and the risk of rollover has been evaluated using the TruckSim ® mechanical simulation software. The shape of the cross sections is (a) one box shaped, (b) one circular and (c) two ellipticals having the same maximum capacity. The scenarios used in the investigation are the tilt table test and a double lane change. Lateral acceleration and roll angle have been monitored in the first scenario and lateral acceleration, roll angle, yaw rate and vertical tire forces have been monitored in the second scenario.

According to the results of the tilt-table test, the safest cross-section is M4 with rollover threshold of 0.39 g. The same conclusion can be drawn also from double lane change scenario where the cross section with the lower risk of rollover is M4 (elliptical) followed by the M1 (box-shaped) that do not rollover in double lane change with constant velocity of 70 km/h. In the double lane change, with constant velocity of 30 km/h, the dynamic responses of all tank cross-sectional geometries are quite similar.

REFERENCES

[1] Information on Statistics Explained (https://ec.europa.eu/eurostat/statistics-explained/index.php?title=Road_freight_transport_by_type_of_goods&oldid=549630#Road_freight_transport_of_dangerous_goods).

[2] National Highway Traffic Safety Administration, Traffic Safety Fact Annual Report, 2016.

[3] Bai, Z.: "Method of Improving Lateral Stability by Using Additional Yaw Moment of Semi Trailer", 2020.

[4] Oberoi, D.: "Enhancing roll stability and directional perfomance of articulated heavy vehicles based on anti-roll control and optimization", 2011.

[5] Xin, T.: „Research on the speed thresholds of trucks in a sharp turn based on dynamic rollover risk levels", 2021.

[6] Shimanovsky, A.: "Dynamics of Tank Trucks with Baffles for Transportation of Viscous Liquids", 2018.

[7] ISO16333. Heavy commercial vehicles and buses-Steady state rollover threshold- Tilt table test method, 2004.

[8] Manual, TruckSim Version 19.0. Mechanical Simulation Corporation, 2018.

[9] EN13094. Tanks for the Transport of DANGEROUS Goods-Metallic Tanks with a Working Pressure not Exceeding 0.5 Bar Design and Construction. British Standards Institution (BSI), London, UK., 2015.

[10] Regulation No. 111. Uniform provisions concerning the approval of tank vehicles of categories n and owith regard to rollover stability, united nations, 2011.

MOBILITY & VEHICLE MECHANICS

https://doi.org/10.24874/mvm.2022.48.03.05
UDC: 67.05;629.3.016.8

MODELING AND SIMULATION OF THE OPERATION OF PHOTOVOLTAIC SYSTEM FOR MEETING ELECTRICITY CONSUMPTION OF RESIDENTIAL HOUSE CONSUMERS, INCLUDING ELECTRIC VEHICLE

Novak Popović [1], Novak Nikolić [2], Nebojša Lukić [3]*

Received in August 2022 *Revised in September 2022* *Accepted in October 2022*
RESEARCH ARTICLE

ABSTRACT: In this paper, the sizing of the solar photovoltaic (PV) system which would meet the total yearly electricity needs of the existing single-family residential house in the territory of the city of Kragujevac (Serbia), was carried out. Two cases were considered. In the first case (case 1), the solar system would produce electricity that corresponds to the actual yearly electricity consumption of the existing electricity consumers in the house. On the other hand, in case 2, the basis for the system sizing would be the sum of the consumption of existing consumers and electricity consumption of the electric vehicle (EV). The energy and economic performance of the house with and without EV load were evaluated. Its energy behavior was simulated for real weather data by using EnergyPlus software. According to the simulation results, the shortest payback period for the installation of the PV system in case 1 is 6 years, and in case 2, for the installation of the PV system and purchasing an EV is 19 years.

KEY WORDS: *PV panel, electricity, electric vehicle, EnergyPlus, simulation*

[1] *Novak Popović, MSc student, University of Kragujevac, Faculty of Engineering, Sestre Janjić 6, 34000 Kragujevac, Serbia, novakpopovickg4@gmail.com (*Corresponding author)*
[2] *Novak Nikolić, PhD Associate professor, University of Kragujevac, Faculty of Engineering, Sestre Janjić 6, 34000 Kragujevac, novak.nikolic@kg.ac.rs, https://orcid.org/0000-0002-3946-0923*
[3] *Nebojša Lukić, PhD Professor, University of Kragujevac, Faculty of Engineering, Sestre Janjić 6, 34000 Kragujevac, Serbia, lukic@kg.ac.rs, https://orcid.org/0000-0002-1923-5200*

MODELIRANJE I SIMULACIJA RADA FOTONAPONSKOG SISTEMA ZA PODMIRIVANJE POTROŠNJE ELEKTRIČNE ENERIJE POTROŠAČA STAMBENE KUĆE KOJI UKLJUČUJU I ELEKTRIČNO VOZILO

REZIME: U ovom radu izvršeno je dimenzionisanje solarnog fotonaponskog (PV) sistema koji bi podmirivao ukupne godišnje potrebe za električnom energijom postojeće jednoporodične stambene kuće na teritoriji grada Kragujevca (Srbija). Razmatrana su dva slučaja. U prvom slučaju (slučaj 1) solarni sistem bi proizvodio električnu energiju koja odgovara stvarnoj godišnjoj potrošnji električne energije postojećih električnih potrošača u kući. S druge strane, kod slučaja 2 osnov za dimenzionisanje sistema bio bi zbir potrošnje postojećih potrošača i potrošnje električne energije električnog vozila (EV). Izvršene su procene energetskog i ekonomskog učinka kuće sa i bez opterećenja EV. Njeno energetsko ponašanje simulirano je za stvarne podatke o vremenskim prilikama upotrebom softvera EnergyPlus. Prema rezultatima simulacija najkraći period otplate troškova ugradnje PV sistema u slučaju 1 iznosi 6 godina, a u slučaju 2, troškova ugradnje PV sistema i kupovine EV, 19 godina.

KLJUČNE REČI: *PV panel, električna energija, električno vozilo, EnergyPlus, simulacija*

MODELING AND SIMULATION OF THE OPERATION OF PHOTOVOLTAIC SYSTEM FOR MEETING ELECTRICITY CONSUMPTION OF RESIDENTIAL HOUSE CONSUMERS, INCLUDING ELECTRIC VEHICLE

Novak Popović, Novak Nikolić, Nebojša Lukić

INTRODUCTION

Electric vehicle (EV) will become an important component of household energy consumption globally under the plans to replace cars based on internal combustion engines [1]. The vehicle electrification is conceived as vehicle efficiency improvement [2]. The EV usage gives new hope that they can represent an alternative that is more likely to support not only the development of sustainable transport, but sustainable development in the broadest sense [3]. Well-built infrastructure for recharging the EV batteries is considered as one of the key issues for the success of the EV, in addition to their price [4]. Many studies indicate that the most important location for EV charging is at home, followed by work, and then public locations. [5]. According to Ref. [6] 45% of the private EV owners say they would charge their EV using renewable energy source either via rooftop solar panels (PV panels) and household battery (31%) or via an electricity contract which utilises green power or carbon offset (14%). The demand of PV panels and EV is expected to increase in the future. An example of their simultaneous growth is represented by the Californian market, where about 40% of EV owners also own solar PV systems [7]. Kobashi and Yarime [8] found that the integration of PV and EV technology would reduce yearly energy costs by 68% and CO2 emissions by 92% in 2030 of households in Japan. Manns [9] conducted a techno-environmental analysis of the German multi-family buildings with rooftop PV systems and EV charging stations. He revealed that 2 to 4 tonnes of CO2-equivalent emissions can be saved annually per residential home, depending on the building size (number of flats). Chowdhury et al. [10] optimized the operation of the existing PV system installed in the Institute of Energy of Dhaka University that would be integrated with the EV. It was concluded that 21% of the total electricity production can be used for EV charging thus reducing greenhouse gas emissions by 52,944 kg/year. The EV charging substantially affects the optimal size of the PV system for self-production and self-consumption of electricity. Piazza et al. [11] considered the impact of the electric mobility on the optimal design of a PV system. The developed optimization model applied to the campus building of the University of Genova demonstrates that the presence of EV increases the optimal size of the PV system from 15% to 25%. Munkhammar et al. [12] studied the impact of the EV charging on the size of a PV system within a net-zero energy building (NZEB) in Sweden. It was revealed that the integration of EV and residential house caused the increase of the yearly household electricity load and PV system size by 37%. Two existing single-family houses located in Netherlands and Belgium that meet NZEB standards (PV system installed) were used to analyze the energy and environmental performance of the building with and without EV load [13]. It was shown that the house with EV load can have 27 to 95% higher energy demands but lower total emissions by 11 to 35%. The effect of EV home charging and PV electricity production on the household electricity use as a future scenario in the city of Westminster was investigated in [14]. According to the obtained results the EV charging leads to the increase of the household electricity use by 14% to 61% depending on the number of occupants. Also, it was pointed out that the EV charging hours should be synchronized with the hours of PV electricity production.

A small-scale PV system could be profitable if its investment costs are low or subsidies are provided [15]. The territory of the Republic of Serbia has quite satisfactory conditions for the exploitation of resources obtained from the Sun, with yearly solar radiation reaching around 1400 kWh/m2 [16]. Low electricity prices in Serbia extend the simple payback period (SPB), making investing in the solar PV system a questionable decision. The incentive in the form of a state subsidy made this procedure more affordable by lowering investment costs and reducing the SPB. Preradović [17] compared the solar energy potential of six different cities, in six different countries, Freiburg (Germany), Graz (Austria), Maribor (Slovenia), Banja Luka (Bosnia and Herzegovina), Niš (Serbia), and Athens (Greece). The results show that Athens has the highest potential for solar energy production with 2108.31 kWh/m2 of yearly solar radiation, and that Niš stands second with 1662.62 kWh/m2. It was concluded that SPB is the shortest for the countries where the electricity price is the highest and vice versa. In other words, in Germany the SPB for installed PV system is the shortest, and in Serbia the longest.

Unfortunately there are no publications concerning the energy and economic viability of a system consisting of the grid-connected rooftop PV and EV within the residential house in the Serbian climatic conditions. The contribution of this paper refers to the answer to the question of whether a small-scale PV system is profitable in the current conditions of the Serbian electricity and EV market. As an example, a household in the city of Kragujevac was chosen. This analysis was carried out for two cases. Case 1 implies the installation of a PV system for a household without EV charging, while case 2 will provide the calculation for the chosen household but which includes EV load. For both cases the size of the PV system and SPB were determined.

1. METHODOLOGY

The software used in this paper enabled the realization of all the necessary tasks. For the creation of the 3D model of a residential building the software "SketchUp2016" was selected [18]. Using the tools of the "Open Studio" software, a 3D model from the "SketchUp2016" was inserted into the "EnergyPlus" software, in which the sizing and simulation of the PV system were carried out [19]. Geometric models of the household buildings were made on the basis of already existing buildings, located on the territory of the city of Kragujevac. They are two separate buildings (Fig. 1), a residential house and an auxiliary building, both consisting of two floors and an attic, and representing the home of a family of five.

The position of the surface on which the PV panels should be installed (roof of the auxiliary building) is determined by orientation of 200˚ and tilt angle of 39.1˚. This angle approximately corresponds to the yearly optimal tilt angle of the solar collector, of 37.5˚, for the city of Kragujevac. The average monthly household electricity consumption, calculated on the basis of the actual electricity bills, is about 500 kWh.

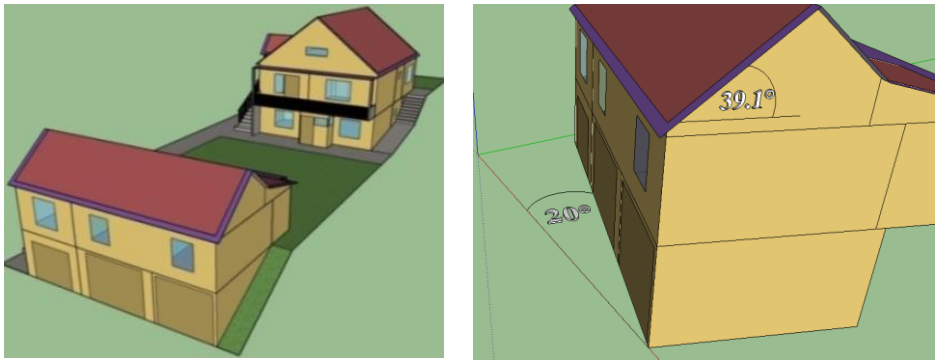

Figure 1. Isometric view of the analyzed residential and auxiliary building (left) and position of the auxiliary building selected for PV system installation (right)

When choosing the EV, an analysis of the entire market was carried out. Preference was given to those with the highest possible range, the highest possible efficiency and the lowest possible price. The analysis was performed for new vehicles that can serve as a family car for a family of five. The vehicle currently owned by the household is "Citroën C4", whose dimensions served as a reference value when choosing an EV. It was decided that the electric car most suitable for this household is the "Volkswagen ID.3 Pro S". The specifications of this car are given in Table 1 [20], while in Fig. 2 its appearance and dimensions are shown.

Table 1. Specifications of the adopted EV [20]

Battery capacity (100%) (kWh)	Useful battery capacity (60%) (kWh)	Average efficiency (Wh)	Range (km)	Top speed (km/h)	Power (kW)	Charging time (100%) (h)	Charging time - fast charger (70%) (h)	Vehicle price (€)
82	49.2	171	450	160	150	8h 15min	71 min	43,603.00

Figure 2. Appearance and dimensions of the adopted EV [21,22]

In order to make the investigation results as comprehensive as possible, the investigation will be conducted in two cases. Case 1 represents a case in which the calculation will be based on the existing current electricity consumption of the residential building without an EV. In Case 2, the total electricity consumption of residential building consumers, which include an EV, is considered.

For the purposes of the PV system sizing, it is necessary to determine the amount of electricity that the system should cover. In order to be able to carry out this procedure, the PV panel was first selected. The PV panel, adopted after market analysis, is a panel from the German manufacturer "LUXOR" under the name "Solar ECO Line HC BF M120 375W" [23]. The adopted average panel efficiency is based on the information provided in the technical documentation. The specifications of the selected PV panel, are presented in Table 2. After choosing the PV panel, it is necessary to draw a surface corresponding to the dimensions of that PV panel (1.755 m × 1.038 m) within the 3D building model. This model is imported into the EnergyPlus software, in which the simulation of the PV panel operation for the period of one year is carried out. To simulate weather conditions of the city of Kragujevac (latitude of 44.02˚N, longitude of 20.92˚E) the EnergyPlus weather file was used. Through simulations, it was obtained that the total yearly produced electricity of the selected panel is 664.57 kWh. This data affects the size of the PV system.

Table 2. Specifications of the adopted PV panel [24]

Power (W)	Efficiency (%)	Average efficiency (%)	Lifetime (years)	Warranty (years)	Temperature range (˚C)	Area (m^2)
375	20.94	19.09	25	15	- 40 to 85	1.82

Unlike case 1, in case 2 the total electricity consumption also depends on the consumption of electricity necessary to charge the battery and drive the EV. Its consumption is determined on the assumption that the vehicle is used for half of the year, i.e. in the winter and summer months, in harsh operating conditions when the heating and air conditioning system is used (ambient temperature lower than -10˚C (winter) and higher than 26˚C (summer)), and the rest of the year in ideal conditions. Due to the lack of data, it was assumed that the behavior of the car battery in winter and summer operating conditions is the same. Ideal conditions imply vehicle operation at an outdoor temperature of 23˚C without operation of the heating and air conditioning system. Car battery capacity is recommended never to be charged above 80% and never discharged below 20%, which reduces the battery capacity by 40% [25]. Also, on the basis of the household needs, it was adopted that the daily distance travelled by car is 40 km (Table 3).

The value of the average yearly consumption for case 2 is calculated according to the data taken from [20]. Data on consumption per kilometer for both harsh and ideal conditions are multiplied by the daily travelled distance, whereby the average daily consumption of the vehicle in these conditions is obtained. The number of days in harsh and ideal conditions is obtained by summing the number of days in the months for which these operating conditions apply. The product of the number of days in certain conditions with the daily consumption for those conditions gives a number that represents the total consumption for part of the year in those conditions, so the sum of consumption in ideal months and consumption in harsh months gives the total yearly consumption in case 2. If the yearly consumption is divided by the number of months, the average monthly consumption of an EV is obtained. Dividing this value by the battery capacity gives the number of charges per month, that is, the time spent on the charger during one month. It is possible to calculate the car range if the battery capacity is divided by the average efficiency of the battery. The average efficiency is determined by dividing the yearly consumption of an EV by the product of the number of days in a year and the distance travelled on a daily basis (Table 3).

Table 3. Calculation of the vehicle operational characteristics (case 2)

Battery capacity (100%) (kWh)	Battery capacity (60%) (kWh)	Daily distance traveled (km)	Consumption per km in ideal conditions (kWh/km) [20]	Daily consumption in ideal conditions (kWh)	Consumption per km in harsh conditions (kWh/km) [20]	Daily consumption in harsh conditions (kWh)
82	49.2	40	0.148	5.92	0.203	8.12
Number of days in ideal conditions	Number of days in harsh conditions	Yearly consumption (kWh)	Average monthly consumption (kWh)	Number of battery charges during a month	Average consumption per km (kWh/km)	Range with full battery (km)
183	182	2561.2	213.43	4.34	0.175	280.46

2. RESULTS AND DISCUSSION

2.1 Size of the PV system

As already explained, the size of the PV system is determined by the total yearly consumed electricity of the considered residential building (for the appropriate case) and the total yearly produced electricity of one PV panel (Table 4). For case 1, it was found that the required number of PV panels is 10 (Fig. 3 (left)). The required number of PV panels in case 2, calculated according to the values of the parameters shown in Tables 3 and 4, is 13 (Fig. 3 (right)) (Table 4). Based on the number of PV panels, the appropriate power of the inverter is adopted, which efficiency is also taken into account during the simulation of the PV system operation (Table 4).

Table 4. Size of the PV system for both cases

Case	Yearly electricity production of one PV panel (kWh)	Total electricity consumption (kWh)	Number of PV panels	Adopted number of PV panels	Inverter power (W)	Inverter efficiency (%)
1	664.57	6027.96	9.07	10	4200 [26]	97.60% [26]
2	664.57	8591.23	12.93	13	5000 [27]	97.50% [27]

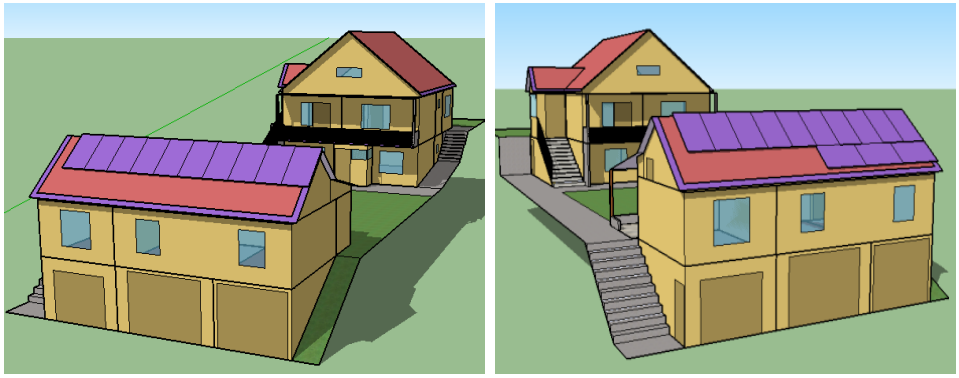

Figure 3. 3D models of a residential house with the required number of PV panels for case 1 (left) and case 2 (right)

Fig. 4 shows a diagram of the electricity production and consumption in both cases. As a reminder, electricity consumption was adopted on the basis of the actual household bills, and it can be concluded that it is the lowest during the summer months and the highest during the winter months. The difference between consumption in case 2 and case 1 corresponds to the amount of electricity needed to charge the EV battery, while the difference in production between these two cases exists because of the higher number of PV panels adopted in case 2. Electricity production in both cases has a completely opposite pattern of behavior in relation to its consumption during the year. The highest production occurs during the summer months, when the intensity of direct solar radiation is high and the share of diffuse radiation in the total radiation is small, while the lowest production is during the winter months. The total amount of produced electricity is 6645.65 kWh, which exceeds the needs for the same by about 600 kWh, while in the second case it is equal to 8639.35 kWh, with a surplus of about 50 kWh.

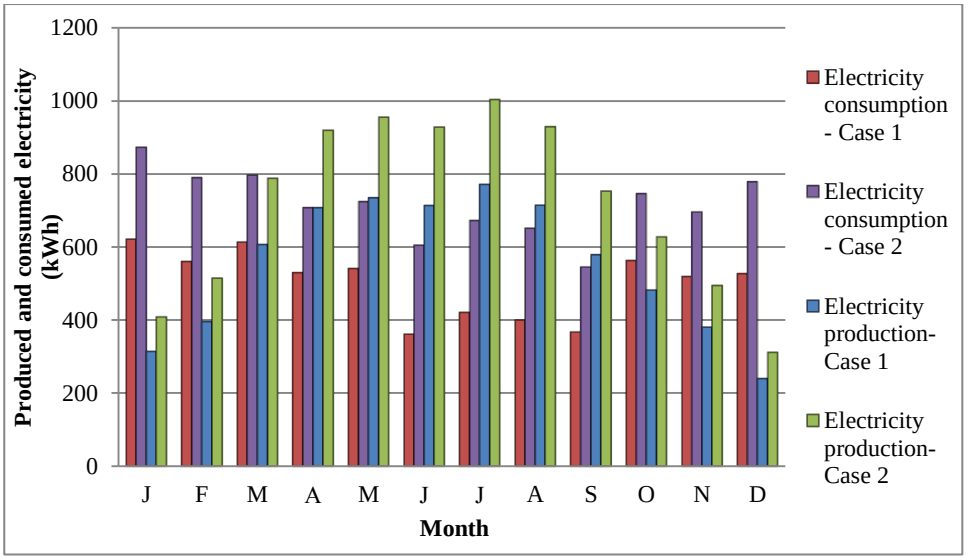

Figure 4. Monthly electricity consumption and production in both considered cases

2.2 Cost-effectiveness analysis

Before analyzing the profitability of installing the system, a couple of terms should be defined. First of all, it is necessary to clarify what is behind the term prosumer. A buyer of electricity who produces electricity from renewable energy sources within his facility, uses the produced electricity to meet his own needs, and hands over the surplus to the network, is called a prosumer. Before becoming a prosumer, the buyer of electricity can apply for a subsidy for the PV system installation. Subsidies represent financial assistance from the state for investments by citizens in which the state has an interest. Subsidies for the installation of PV systems, provided by the Republic of Serbia, cover 50% of the total investment costs, with the condition that the maximum power of the system for which these privileges can be realized is 6 kW [28]. It is also important to note that in case 2, the right to a subsidy for purchasing an EV, which amounts to €5,000.00 for the fully EV, can be earned, too [29].

In Table 5 the yearly costs of electricity after the PV system installation are given. Based on the actual consumption bills, total household electricity costs amount to 40,208.00 RSD. These costs are calculated without including additional costs in the form of fees to the supplier. As they do not disappear after the installation of the PV system and it is impossible to predict them, for the purposes of this work, their influence is not considered. The principle of calculating electricity costs after installing a PV system is as follows. In months when consumption exceeds production, electricity costs will be calculated based on the amount of electricity consumed under the lower tariff increased by the difference between the electricity consumed under the higher tariff and the electricity produced.

The electricity prices of the corresponding zone in the corresponding tariff are adopted according to [30]. In months when production exceeds consumption, or they are equal, electricity costs will be calculated based on the electricity consumed within the lower tariff. According to [31], the unused part of electricity can be carried over to the next month and used in months when the production does not meet the consumption until 1st of April of the next year.

Table 5 Monthly electricity costs in both considered cases (1 € = 118 RSD)

Month	Production (kWh)		Consumption- higher tariff (kWh)		Consumption- lower tariff (kWh)		Difference between produced and consumed electricity at the end of the month (kWh)		Cost of electricity for both cases (RSD)
	Case 1	Case 2	Case 1	Case 2	Case 1	Case 2	Case 1	Case 2	
A	708	920	406	584	124	124	302	337	267.22
M	735	955	404	588	137	137	633	704	295.24
J	714	929	276	520	86	86	1071	1113	185.33
J	772	1004	400	652	21	21	1443	1466	45.26
A	715	930	326	578	74	74	1832	1818	159.47
S	579	753	302	480	66	66	2109	2092	142.23
O	483	628	450	634	113	113	2142	2086	243.515
N	381	495	403	581	116	116	2120	2001	249.98
D	240	312	395	647	132	132	1965	1666	284.46
J	314	409	486	738	136	136	1793	1337	293.08
F	396	515	439	668	122	122	1750	1184	262.91
M	607	789	464	648	150	150	1893	1325	323.25
Sum	6646	8639	4751	7314	1277	1277	1893	1325	2,751.95

From Table 5 and Fig. 4, it can be concluded that electricity production meets consumption in all months. The calculation results also indicate a problem related to the system oversizing. Guided by the idea that the system should have as many solar panels as necessary to meet the yearly electricity consumption, a mistake is being made. Since the produced electricity can be used only in the tariff in which it was produced, which is certainly only within the higher tariff, the electricity consumed in the lower tariff should then be excluded from the calculation. Also, according to [20], after 1st of April all the unused electricity is actually "gifted" to electricity provider, which further complicates the system sizing. From the table above, it can be concluded that the system is oversized in the first case by almost 3 PV panels and in the second by almost 2 PV panels. Investment costs for both cases are given in Table 6.

Table 6 Investment costs for both considered cases in thousands of RSD (1 € = 118 RSD)

PV panel price (in 000 RSD) [24]		Inverter price (in 000 RSD) [26][27]		Roof truss price (in 000 RSD) [32]		Price of other elements and system mounting (in 000 RSD) [33]		Price of smart electricity meter (in 000 RSD) [34]		Price of EV with subsidy (in 000 RSD) [20]	
Case											
1	2	1	2	1	2	1	2	1	2	1	2
220.66	286.86	75.00	118.80	38.72	52.34	65.00		44.35		0	5,113.52

According to Table 6, the total cost of installing the PV system for case 1 is 443,735.00 RSD without subsidy and 221,867.50 RSD with subsidy. In case 2, the installation cost without subsidy amounts to 5,094,493.92 RSD, and with the subsidy for the installation of the PV system, 4,810,821.42 RSD. The subsidy for buying the selected EV is 586,372.68 RSD [29]. A few more things need to be emphasized. As the EV is charged using electricity produced within the home, its charging is free (if the vehicle is charged within a higher tariff). Therefore, the fuel savings are equal to the yearly fuel costs for the currently used household car, which are 190,530.00 RSD. Also, the price of the EV, which is a replacement for the mentioned vehicle, can be reduced by the market value of that car, which is 410,789.00 RSD. When all the necessary parameters are calculated, the SPB can be determined. For case 1, the SPB without the participation of the state in the form of subsidy for the installation of solar PV system is 11 years, 10 months and 4 days, while with the subsidy it is 5 years, 11 months and 2 days. For case 2, the SPB without the subsidy amounts to 20 years, 6 months and 15 days, while with the subsidy it amounts to 19 years, 3 months and 18 days.

3. CONCLUSIONS

In this paper, the sizing of the solar PV system which would meet the total yearly electricity needs of a residential house in the territory of the city of Kragujevac, was carried out. Two cases were considered. In the first case (case 1), the solar system would produce electricity that corresponds to the actual yearly electricity consumption of the existing electricity consumers in the house. On the other hand, in case 2, the basis for the system sizing would be the sum of the consumption of existing consumers and electricity consumption of the EV. Sizing was preceded by the creation of a 3D house model in the software "SketchUp2016" and a PV panel model in the software "EnergyPlus", in which its energy behavior was simulated for real weather data for the city of Kragujevac. According to the simulation results, the shortest payback period for the installation of the PV system in case 1 is 6 years, and in case 2, for the installation of the PV system and purchasing an EV is 19 years.

Certain assumptions were adopted before making the calculations. The efficiency of the solar PV panel of 19.09% is adopted as average and constant for 25 years, which means that in the first half of its lifetime the efficiency of this panel will be slightly lower, while in the second half it will be higher. In reality, it will be lower and variable due to operating conditions that differ from the test conditions of the PV panel. In this regard, the influence of temperature and soiling of the receiving surface of the panel on its efficiency was neglected. Also, it was adopted that the habits of the householders do not change. After installing the PV system, using the large electricity consumers within the lower tariff becomes the most unprofitable option. Regarding case 2, it can be noticed that EV prices still are not low enough, or in other words, the efficiency and range of cheaper ones are not yet satisfactory. Since it is a still rising technology, a drop in the price and an improvement in the car characteristics can be expected. Also, the PV panel technology development is on the rise, so in the future their profitability for both cases could be shorter.

According to the currently available data on electricity bills, recently sent to households that received the status of prosumer, it seems that the sizing of the PV system according to the total yearly electricity needs is wrong, that is, the system is oversized. The reason for this lies in the calculation of electricity consumption within the lower tariff and the fact that the prosumer loses the possibility of using "accumulated" electricity produced from previous months after 31st of March. The solution to this problem would be a

purposeful increase in electricity consumption by installing electric heating systems (heat pump...), where the investment would pay off in another field. On the other hand, a potential solution to the problem would be the possibility of calculating the "accumulated" produced electricity in the next accounting period or meeting the electricity consumed in a lower tariff (at night), with the cancellation or reduction of the corresponding fees. Due to the impossibility of determining the amount of fees and charges that increase the amount of the bill, there was not much to say about it in this paper, and the problems and advantages related to it remain the subject of some subsequent research.

4. REFERENCES

[1] International Energy Agency. Global EV Outlook 2020. (2020). Available: https://www.iea.org/reports/global-ev-outlook-2020 (accessed 10.07.2022.)

[2] Belingardi, G., Amati, N., & Bonfitto, A.: ELECTRIC AND HYBRID VEHICLES: ARE WE READY FOR THE NEW MOBILITY ERA?; vol. 47, no. 2, Mobility & Vehicle Mechanics, 2021.

[3] Kjosevski, S., Kochov, A., Kostikj, A.: AN INDICATORS BASED APPROACH TOWARDS DECISION MAKING AND POLICY MAKING REGARDING INTRODUCING ELECTRIC VEHICLES; vol. 45, no. 4, Mobility & Vehicle Mechanics, 2019.

[4] Gruden, D.: WILL ELECTRIC MOTOR SUBSTITUTE INTERNAL COMBUSTION ENGINE?; vol. 45, no. 4, Mobility & Vehicle Mechanics, 2019.

[5] Hardman, S., Jenn, A., Tal, G., Axsen, J., Beard, G., Daina, N., ... & Witkamp, B.: A review of consumer preferences of and interactions with electric vehicle charging infrastructure.; vol.62, 508-523, Transportation Research Part D: Transport and Environment, 2018.

[6] Electric Vehicle Council. State of Electric Vehicles. (2020). Available: https://electricvehiclecouncil.com.au/reports/state-of-electric-vehicles-2020/ (accessed 12.06.2022.)

[7] Buonomano, A.: Building to Vehicle to Building concept: A comprehensive parametric and sensitivity analysis for decision making aims.; vol. 261, 114077 Applied Energy, 2020.

[8] Kobashi, T., & Yarime, M.: Techno-economic assessment of the residential photovoltaic systems integrated with electric vehicles: A case study of Japanese households towards 2030.; vol. 158, 3802-3807, Energy Procedia, 2019.

[9] Manns, P. (2019). A techno-environmental analysis on the effect of combining EV charging stations with PV tenant law systems and subsidies on the reduction of greenhouse gas emissions. Available: https://www.researchgate.net/publication/341151178 (accessed 18.07.2022.)

[10] Chowdhury, N., Hossain, C. A., Longo, M., & Yaïci, W.: Optimization of solar energy system for the electric vehicle at university campus in Dhaka, Bangladesh. vol. 11(9), 2433. Energies, 2018.

[11] Piazza, G., Bracco, S., Delfino, F., Di Somma, M., & Graditi, G.: Impact of electric mobility on the design of renewable energy collective self-consumers.; 100963 Sustainable Energy, Grids and Networks, 2022.

[12] Munkhammar, J., Grahn, P., & Widén, J.: Quantifying self-consumption of on-site photovoltaic power generation in households with electric vehicle home charging. vol. *97*, 208-216, *Solar energy*, 2013.

[13] Rehman, H. U., Diriken, J., Hasan, A., Verbeke, S., & Reda, F.: Energy and Emission Implications of Electric Vehicles Integration with Nearly and Net Zero Energy Buildings. vol. *14*(21), 6990, *Energies*, 2021.
[14] Munkhammar, J., Bishop, J. D., Sarralde, J. J., Tian, W., & Choudhary, R.: Household electricity use, electric vehicle home-charging and distributed photovoltaic power production in the city of Westminster. vol. *86*, 439-448, *Energy and Buildings*, 2015.
[15] Koskela, J., Rautiainen, A., & Järventausta, P.: Using electrical energy storage in residential buildings–Sizing of battery and photovoltaic panels based on electricity cost optimization. vol. *239*, 1175-1189, *Applied energy*, 2019.
[16] Pavlovic, T. (Ed.).: *The Sun and Photovoltaic Technologies*. Springer Nature, 2019.
[17] Preradović, M.: Solar energy potential in Freiburg, Graz, Maribor, Banja Luka, Niš, and Athens. vol. *35*(3), 393-403 *Facta Universitatis, Series: Electronics and Energetics*, 2022.
[18] https://www.sketchup.com/try-sketchup (accessed 20.08.2022.)
[19] http://nrel.github.io/OpenStudio-user-documentation/ (accessed 20.08.2022.)
[20] https://ev-database.org/car/1534/Volkswagen-ID3-Pro-S---5-Seats (accessed 23.08.2022.)
[21] https://insideevs.com/news/401952/more-details-vw-id3-revealed/ (accessed 23.08.2022.)
[22] https://vrelegume.rs/prva-voznja-i-utisci-volkswagen-id-3/ (accessed 23.08.2022.)
[23] https://www.suncica.co.rs/solarni-paneli-i-oprema/solarni-paneli/solarni-monokristalni-panel-luxor-410w-hlafcut.html (accessed 23.08.2022.)
[24] https://www.suncica.co.rs/pub/media/wysiwyg/Luxor_375W.pdf (accessed 22.08.2022.)
[25] https://dmotion.rs/2021/03/10/koliko-su-izdrzljive-baterije-u-elektricnim-automobilima/ (accessed 23.08.2022.)
[26] https://www.solar-shop.rs/proizvodi/solarni-on-grid-inverter-growatt-mic-3000-tl-x/ (accessed 22.08.2022.)
[27] https://www.solar-shop.rs/proizvodi/solarni-on-grid-pretvarac-growatt-min-5000tl-xe/ (accessed 22.08.2022.)
[28] https://balkangreenenergynews.com/rs/raspisan-konkurs-za-subvencije-za-solarne-panele-za-domacinstva-u-deset-gradova-u-srbiji/ (accessed 29.08.2022.)
[29] https://plutonlogistics.com/drumski-transport/subvencije-za-kupovinu-elektricnih-i-hibridnih-vozila-i-u-2022-podsticaji-do-5-000-evra/ (accessed 29.08.2022.)
[30] https://www.eps.rs/cir/snabdevanje/Documents/20220722_Odluka%20o%20ceni.pdf (accessed 30.08.2022.)
[31] https://balkangreenenergynews.com/rs/srbija-usvojila-uredbu-o-prozjumerima-u-tri-koraka-do-struje-iz-solarnih-panela/ (accessed 24.08.2022.)
[32] https://www.solarni-paneli.co.rs/pdf/cenovnik-solarnih-panela.pdf (accessed 22.08.2022.)
[33] https://www.suncica.co.rs/solarni-sistemi/on-grid-solarni-sistemi.html (accessed 30.08.2022.)
[34] https://qubino.com/products/3-phase-smart-meter/#buy3phasesmartmeter (accessed 30.08.2022.)

MVM – International Journal for Vehicle Mechanics, Engines and Transportation Systems

NOTIFICATION TO AUTHORS

The Journal MVM publishes original papers which have not been previously published in other journals. This is responsibility of the author. The authors agree that the copyright for their article is transferred to the publisher when the article is accepted for publication.

The language of the Journal is English.

Journal ***Mobility & Vehicles Mechanics*** is at the SSCI list.

All submitted manuscripts will be reviewed. Entire correspondence will be performed with the first-named author.

Authors will be notified of acceptance of their manuscripts, if their manuscripts are adopted.

INSTRUCTIONS TO AUTHORS AS REGARDS THE TECHNICAL ARRANGEMENTS OF MANUSCRIPTS:

Abstract is a separate Word document, "*First author family name_ABSTRACT.doc*". Native authors should write the abstract in both languages (Serbian and English). The abstracts of foreign authors will be translated in Serbian.

This document should include the following: 1) author's name, affiliation and title, the first named author's address and e-mail – for correspondence, 2) working title of the paper, 3) abstract containing no more then 100 words, 4) abstract containing no more than 5 key words.

The manuscript is the separate file, „*First author family name_Paper.doc*" which includes appendices and figures involved within the text. At the end of the paper, a reference list and eventual acknowledgements should be given. References to published literature should be quoted in the text brackets and grouped together at the end of the paper in numerical order.

Paper size: Max 16 pages of B5 format, excluding abstract
Text processor: Microsoft Word
Margins: left/right: mirror margin, inside: 2.5 cm, outside: 2 cm, top: 2.5 cm, bottom: 2 cm
Font: Times New Roman, 10 pt
Paper title: Uppercase, bold, 11 pt
Chapter title: Uppercase, bold, 10 pt
Subchapter title: Lowercase, bold, 10 pt
Table and chart width: max 125 mm
Figure and table title: Figure _ (Table _): Times New Roman, italic 10 pt

Manuscript submission: application should be sent to the following e-mail:

mvm@kg.ac.rs ; lukicj@kg.ac.rs
or posted to address of the Journal:
University of Kragujevac – Faculty of Engineering
International Journal M V M
Sestre Janjić 6, 34000 Kragujevac, Serbia

The Journal editorial board will send to the first-named author a copy of the Journal offprint.

MVM – International Journal for Vehicle Mechanics, Engines and Transportation Systems

OBAVEŠTENJE AUTORIMA

Časopis MVM objavljuje orginalne radove koji nisu prethodno objavljivani u drugim časopisima, što je odgovornost autora. Za rad koji je prihvaćen za štampu, prava umnožavanja pripadaju izdavaču.

Časopis se izdaje na engleskom jeziku.

Časopis ***Mobility & Vehicles Mechanics*** se nalazi na SSCI listi.

Svi prispeli radovi se recenziraju. Sva komunikacija se obavlja sa prvim autorom.

UPUTSTVO AUTORIMA ZA TEHNIČKU PRIPREMU RADOVA

Rezime je poseban Word dokument, "*First author family name_ABSTRACT.doc*". Za domaće autore je dvojezičan (srpski i engleski). Inostranim autorima rezime se prevodi na srpski jezik. Ovaj dokument treba da sadrži: 1) ime autora, zanimanje i zvanje, adresu prvog autora preko koje se obavlja sva potrebna korespondencija; 2) naslov rada; 3) kratak sažetak, do 100 reči, 4) do 5 ključnih reči.

Rad je poseban fajl, „*First author family name_Paper.doc*" koji sadrži priloge i slike uključene u tekst. Na kraju rada nalazi se spisak literature i eventualno zahvalnost. Numeraciju korišćenih referenci treba navesti u srednjim zagradama i grupisati ih na kraju rada po rastućem redosledu.

Dužina rada: Najviše 16 stranica B5 formata, ne uključujući rezime
Tekst procesor: Microsoft Word
Margine: levo/desno: mirror margine; unurašnja: 2.5 cm; spoljna: 2 cm, gore: 2.5 cm, dole: 2 cm
Font: Times New Roman, 10 pt
Naslov rada: Velika slova, bold, 11 pt
Naslov poglavlja: Velika slova, bold, 10 pt
Naslov potpoglavlja: Mala slova, bold, 10 pt
Širina tabela,dijagrama: max 125 mm
Nazivi slika, tabela: Figure __ (Table _): Times New Roman, italic 10 pt

Dostavljanje rada elektronski na E-mail: **mvm@kg.ac.rs ; lukicj@kg.ac.rs**

ili poštom na adresu Časopisa
Redakcija časopisa M V M
Fakultet inženjerskih nauka
Sestre Janjić 6, 34000 Kragujevac, Srbija

Po objavljivanju rada, Redakcija časopisa šalje prvom autoru jedan primerak časopisa.

MVM *Editorial Board*
University of Kragujevac
Faculty of Engineering
Sestre Janjić 6, 34000 Kragujevac, Serbia
Tel.: +381/34/335990; Fax: + 381/34/333192
www.mvm.fink.rs